BIOPERIANT12: a ~~mesoscale resolving~~ mesoscale-resolving coupled ~~physics-biogeochemical~~ physics–biogeochemical model for the Southern Ocean

Nicolette Chang[1,2], Sarah-Anne Nicholson[1], Marcel du Plessis[3], Alice D. Lebehot[1], Thulwaneng Mashifane[1], Tumelo C. Moalusi[1,2], N. Precious Mongwe[1,4], and Pedro M.S. Monteiro[1,2,5]

[1]Southern Ocean Carbon-Climate Observatory, CSIR, Cape Town, South Africa
[2]Global Change Institute, University of the Witwatersrand, Johannesburg, South Africa
[3]Department of Marine Science, University of Gothenburg, Sweden
[4]Geosciences Department, Princeton University, Princeton, New Jersey, USA
[5]School for Climate Studies, Stellenbosch University, Stellenbosch, South Africa

Correspondence: Nicolette Chang (nchang@csir.co.za)

Abstract. We present BIOPERIANT12, a regional 1/12° ocean–ice–biogeochemical model configuration of the Southern Ocean ~~(SO) at a mesoscale-resolving 1/12. This is a stable, ocean–ice–biogeochemical configuration derived from~~ based on the Nucleus for European Modelling of the Ocean ~~(NEMO) modelling~~ platform. It is ~~specifically~~ designed to investigate ~~questions related to the~~ mean state, seasonal cycle~~variability and mesoscale processes in the mixed layer and within the~~, and upper ocean (< ~~1000 m) . In particular, the focus is on understanding processes behind carbonand~~ 500 m) dynamics, with a particular focus on processes influencing carbon, heat exchange, ~~systematic errors in biogeochemistry and assumptions underlying the parameters chosen to represent these SO processes. The dynamics of the ocean model play a large role in driving ocean biogeochemistry and we show that over the chosen period of analysis~~ biogeochemical mechanisms, and the assumptions underlying physical–biogeochemical model parameterisations within the Southern Ocean. Over the analysis period 2000–2009~~that the simulated dynamics in the upper ocean provide a stable mean state, as~~ , the model demonstrates a stable and realistic upper ocean mean state compared to observation-based ~~datasets (themselves subject to biases such as sparsity of data, cloud cover, etc.), and through which the characteristics of variability can be described. Using~~ products. We use ocean biomes to delineate the major ~~regions of the SO, the modeldemonstrates a useful representation of ocean biogeochemistry~~ subregions and evaluate the biogeochemical properties of the model, including surface chlorophyll and partial pressure of carbon dioxide~~(p). In addition to a reasonable model mean state performance, through model–data metrics~~ . BIOPERIANT12 ~~highlights several pathways for improving Southern Ocean model simulations such as the representation of temporal variability and the overestimation of biological biomass~~captures key spatial and temporal features of Southern Ocean biogeochemistry, though it tends to overestimate biological biomass and underrepresents high-frequency variability. The model shows skill in reproducing large-scale patterns and seasonal cycles across biomes, offering insights into regional dynamics that are often obscured in coarser models. Despite its limitations, BIOPERIANT12 provides a valuable high-resolution framework for process studies, model–data intercomparisons, and future investigations into mesoscale influences on carbon and heat dynamics. It offers a useful tool for addressing long-standing uncertainties in air–sea exchange and ecosystem variability in the Southern Ocean.

1 Introduction

The Southern Ocean (SO) is ~~an essential sink of~~ a key region in the global carbon cycle, serving as a major sink for both carbon dioxide (CO_2) and heat~~, responsible~~. It accounts for nearly 40 % of the ~~global ocean annual mean~~ annual mean oceanic CO_2 uptake and 75 % of the ~~excess heat globally (Frölicher et al., 2015; Gruber et al., 2023). Since the 2000s, this sparsely observed region has been increasingly sampled (Williams et al., 2018; Meredith et al., 2013; Swart et al., 2012). These efforts, conducted at increasing~~ global excess heat (Frölicher et al., 2015; Gruber et al., 2023). However, the SO remains a challenging region to both observe and simulate. The recognised sparsity of observations in this dynamic, remote area has been addressed through expanded sampling efforts since the 2000s (Williams et al., 2018; Meredith et al., 2013; Swart et al., 2012). Owing to improvements in sampling technology, data is now being collected at unprecedented temporal and spatial resolutions~~, have exposed the challenge of accurately representing~~. Despite this progress, the data remain weakly constrained and seasonally biased. Model–data comparisons have thus underscored the need to improve the representation of CO_2 ~~heat fluxes of the SO within~~ and heat fluxes in ocean models and ~~by extension, earth~~ Earth system models (ESMs) ~~from which projections are made (Rintoul, 2018), despite being weakly constrained and seasonally biased themselves. The seasonal cycle is arguably the dominant mode of variability in physical-biogeochemical properties of the SO (Lenton et al., 2013; Thomalla et al., 2011; Mongwe et al., 2~~ , yet the state-of-the-art, particularly the ocean components of ESMs (Chassignet et al., 2020; Treguier et al., 2023), display ~~inadequate representation of these scales. Large model biases in ESMs are seen in the wide, inter-model spread of the contributing models in the previous generations of Climate Model Intercomparison Project (CMIP). This is particularly evident in the pronounced inability to reproduce similar seasonal cycles of air-sea~~ used for future climate projections (Rintoul, 2018).

Model ocean dynamics are fundamental to accurately reproducing CO_2 ~~flux (F) (Anav et al., 2013; Lenton et al., 2013; Kessler and Tjipu~~ , sea–ice extent and trends (Meijers, 2014; Beadling et al., 2020), mixed layer depth (MLD) (Sallée et al., 2013; Treguier et al., 2023) , water mass properties (Downes et al., 2015; Beadling et al., 2020), dissolved iron (Tagliabue et al., 2016) and phytoplankton phenology (Thomalla et al., 2011, 2023; Hague and Vichi, 2018). Key to reproducing the heat and heat fluxes in the SO, ~~are the representation of the dynamics in models, particularly the ubiquity of mesoscale eddies~~ particularly due to the ~~strong baroclinically induced instabilities of~~ prevalent mesoscale eddy field driven by the Antarctic Circumpolar Current (ACC) and its associated strong mesoscale kinetic energy and baroclinic instabilities (Daniault and Ménard, 1985; Smith et al., 2023). Mesoscale dynamics ~~explain~~ account for a substantial portion of ~~the~~ both annual and seasonal variance in ~~mixed-layer depths (Whitt et al., 2019; Gaube et al., 2019), and therefore influence global circulation by impacting~~ mixed layer depth (MLD) (Whitt et al., 2019; Gaube et al., 2019), thereby influencing global circulation through water mass transformation and ~~influencing the~~ SO overturning circulation ~~through~~ via eddy compensation and ~~sensitivity of wind (Abernathey et al., 2016; Munday et al., 2~~ . Mesoscale and also submesoscale dynamics, through enhancements in ocean–wind interactions (Abernathey et al., 2016; Munday et al., 20 . Subsequently, enhanced advection and mixing ~~, consequently influence the~~ by mesoscale (and submesoscale) processes impact local biogeochemistry (BGC) ~~and thus carbon exchange, such as by altering~~ through the supply of limiting nutrients to the euphotic layer (Frenger et al., 2015; Nicholson et al., 2019; Uchida et al., 2019) and ~~available light via~~ by modifying light availability through stratification caused by "eddy slumping~~" induced stratification~~ " during spring (Lévy

et al., 1998, 1999; Marshall et al., 2002; Lévy et al., 2010; Mahadevan et al., 2012). ~~Simulations with coupled physics-BGC in global (Rohr et al., 2020) and regional ocean models (Song et al., 2018; Uchida et al., 2019, 2020) show the variability in both biological and physical mechanisms due to eddies influence the biological response~~

Within the framework of the seasonal cycle, arguably the dominant mode of variability in physical–biogeochemical properties of the SO (Lenton et al., 2013; Thomalla et al., 2011; Mongwe et al., 2018; Gregor et al., 2019; Rodgers et al., 2023), ocean models continue to show inadequate representation of SO dynamics (Chassignet et al., 2020; Treguier et al., 2023). This leads to large model biases in ESMs and a wide inter-model spread in previous generations of the Climate Model Intercomparison Project (CMIP). For example, models show divergent seasonal cycles in air–sea CO_2 flux (FCO_2), (Anav et al., 2013; Lenton et al., 2013; Kessler a , sea ice extent and trends (Meijers, 2014; Beadling et al., 2020), MLD (Sallée et al., 2013; Treguier et al., 2023), water mass properties (Downes et al., 2015; Beadling et al., 2020), dissolved iron concentrations (Tagliabue et al., 2016), and phytoplankton phenology (Thomalla et al., 2011, 2023; Hague and Vichi, 2018).

The representation of mesoscale dynamics in ocean models is therefore a critical step toward improving the simulation of CO_2 and heat fluxes. Coupled physics–biogeochemistry (BGC) simulations, in both global (Rohr et al., 2020) and regional models (Song et al., 2018; Uchida et al., 2019, 2020), demonstrate that model resolution strongly influences biological responses in the SO~~with implications both spatially and temporally, such as in the characteristics of the seasonal cyclesof both physical and BGC processes. Computational cost is still a limiting factor in the design of both projection and process models ; while computational power(and horizontal model resolution) has increased~~ . These effects arise through more refined representations of both physical and biogeochemical mechanisms, particularly in the structure and timing of seasonal cycles. However, the ability to resolve such processes is limited by computational costs, especially in models that include BGC components. BGC can add substantially to the overall cost which increases with the number of BGC tracers that must be advected and the complexity of numerical schemes employed (Lévy et al., 2012). For long-running coupled models designed to address climate-scale questions, lower resolutions are thus often used. This choice contributes to uncertainties in simulating carbon and heat exchange (Hewitt et al., 2020; Beadling et al., 2020). Despite gains in computational power, demonstrated by the shift from CMIP5 ~~(resolutions of~~ models with horizontal resolutions coarser than 1° ~~or coarser and relied on suitable parameterisations),~~ to CMIP6 ~~only has resolutions of up~~ models of up to 0.25° ~~which allows some explicit representation of the ocean (Hewitt et al., 2020; Haars , these do not include the mesoscale . Model configurationswith BGC, therefore, compromise in spatial /temporal resolutionor run duration~~, most ESMs still do not explicitly resolve mesoscale processes in the SO (Hewitt et al., 2020; Haarsma et al., 2016) .

To balance computational constraints, model configurations, especially those incorporating BGC, must make trade-offs in spatial and temporal resolution, run duration, and model complexity. For ~~example, the MOMSO configuration (Modular Ocean Model Sout is eddy-resolving in the SO (11 km resolution at 40~~simulations focused on SO CO_2 ~~S) but has a reduced BGC model (BLING) consisting of 4 BGC tracers and a carbon module for climatologically forced, multi-decadal experiments. SO iron supply experiments by Uchida et al. (2019), on the other hand, use a full BGC model with phytoplankton and zooplankton functional groups, but an idealised ocean of 20 km resolution, flat-bottomed, re-entrant channel. BGC data assimilation for SO flux experiments in B-SOSE (Biogeochemical Southern Ocean State Estimate) uses model resolution (1/3°, Verdy and Mazloff, 2017, and 1/6°,~~

and run duration which relies on periods of sufficient observations. These configuration compromises contribute to uncertainties in carbon and heat exchange, particularly for climate-scale questions using long-running models (Hewitt et al., 2020; Beadling et al., 2020) . The importance of model resolution is apparent through, firstly, the representation of ocean dynamics that and heat fluxes,
95 resolution is critical: it defines the spatial scales over which ocean dynamics operate to distribute BGC tracersin the model and are the major driver of the BGC differences of simulations with observations and between simulations in ESMs, for , and significantly contributes to model–observation discrepancies. For example, mesoscale modulations modulation of the MLD affect affects light and iron supply to surfaceinfluencing availability at the surface, which in turn influences phytoplankton growth and thus the the strength of the biological carbon pump (Song et al., 2018). Secondly, resolution affects the evolution of
100 the tracers themselves, (Séférian et al., 2013) discuss errors in the BGC fieldswhich may propagate spatially and amplify during model evolution in low resolution simulations, particularly the pools of nutrients and iron which supply the surface, although this matters more for simulations of hundreds of years versus the short model duration of BIOPERIANT12. To understand the heat and carbon biases in SO models, we focus on understanding the biophysical dynamics in the ocean surface mixed-layer, the boundary across which atmosphere-ocean exchange occurs. In addition, low-resolution models are more prone to cumulative
105 errors in BGC fields, such as nutrient and iron pools, which can propagate and amplify over time (Séférian et al., 2013).

In this paper, we present a regional, we present our regional SO model configuration of a laterally unconstrained Antarctic Circumpolar Current (ACC) with resolved eddies and a prescribed atmosphere. BIOPERIANT12 is a regional, circumpolar, mesoscale-resolving (1/12°), contemporary ocean–ice–biogeochemical, NEMO–PISCES model configuration,), contemporary ocean–ice–BGC model configuration using NEMO–PISCES. The PISCES biogeochemical model simulates 24 evolving prognostic
110 tracers for carbon and nutrients cycles, as well as marine productivity, with two phytoplankton groups (nanophytoplankton and diatoms) and two zooplankton groups (microzooplankton and mesozooplankton) (Aumont and Bopp, 2006; Aumont et al., 2015) . This setup allows us to examine: the seasonal cycle of physical and biogeochemical processes in the surface ocean, the interface across which atmosphere–ocean exchange occurs; model–observation biases through comparison with in situ data; and simulation development through applications such as downscaling, submesoscale experiments, and sensitivity studies.

115 More specifically, BIOPERIANT12 . This configuration has a laterally unconstrained ACC with resolved eddies, and a prescribed atmosphere to evolve the SOover a limited duration allows the investigation of how sub-seasonal to synoptic-scale atmospheric forcing, such as storms, modulates seasonal buoyancy fluxes in an eddying ocean, and how these interactions shape BGC and carbon fluxes. Observational campaigns, including those with gliders, show storm events are key drivers of biological variability by influencing processes such as vertical mixing, nutrient supply, and light availability (Nicholson et al., 2022; Toolsee et al., 202
120 , yet these processes are not resolved in most ESMs. BIOPERIANT12's mesoscale-resolving resolution makes it well-suited to investigate these biophysical processes.

For comparison, the MOMSO configuration (Modular Ocean Model–Southern Ocean; Dietze et al. (2020)) is also eddy-resolving in the SO (11 km resolution at 40 °S), used in climatologically forced, multi-decadal experiments, but uses a reduced BGC model (BLING) with only four tracers and a simplified carbon module. Another example, the B-SOSE (Biogeochemical
125 Southern Ocean State Estimate), balances the model complexity of BGC data assimilation with coarser horizontal resolutions (1/3°, Verdy and Mazloff, 2017, and 1/6°, http://sose.ucsd.edu/). The challenge of examining coupled SO dynamics and BGC

is illustrated by the model design of Uchida et al. (2019). In order to examine mesoscale and submesoscale influences on iron fluxes in the SO, they employed a full BGC model with multiple phytoplankton and zooplankton functional groups in experiments at increasing resolutions (20~~years)~~, 5, and 2 km), each requiring a spin-up. However, to extricate the influence of resolved, evolving ocean dynamics, and thus controlling the underlying ocean, they used an idealised ocean setup represented by a flat-bottomed, re-entrant channel.

While these configurations offer valuable insights into SO dynamics and BGC, their design choices reflect specific research objectives and therefore make them less suited for addressing processes and model representation of SO BGC coupled to realistic mesoscale dynamics that drive the observed variability and air–sea exchange.

This paper is structured as follows: Section 2 provides a description of the model design. ~~We describe the model design in Section 2 .~~ In Section 3, we ~~assess the configurationlooking at model stability and, through a comparison against observations, suitability to serve~~ evaluate the configuration's suitability as an experimental platform~~and for downscaling, submesoscale experiments and sensitivity studies coinciding with in situ experiments (Swart et al., 2012; du Plessis et al., 2022; Djeutchouang et al., 2022 .~~, starting with an assessment of model stability (i.e., whether a stable mean state is achieved) and followed by an evaluation of the BGC seasonal cycle, comparing it with observation-based gridded climatologies. Finally, Section 4 presents the conclusions.

2 BIOPERIANT12 model configuration

BIOPERIANT12 (full configuration name: BIOPERIANT12-CNCLNG01) is a regional, mesoscale-resolving ~~configuration for simulating~~ model configuration designed to simulate the ocean, sea ice, and biogeochemistry of the circumpolar SO ~~for~~ under contemporary conditions. ~~NEMO-PISCES~~ It is based on NEMO–PISCES version 3.4 (Gurvan et al., 2019)~~with specifications by~~ , following specifications from the DRAKKAR consortium (Barnier et al., 2014)~~was used. This consists of an ocean-ice component provided by the~~ . The configuration couples the ocean component OPA (Océan Parallélisé)~~model and Louvain-la-Neuve~~ , the Louvain–la–Neuve Sea Ice Model (LIM2)~~and biogeochemical components by~~ , and the biogeochemical model PISCES (Aumont and Bopp, 2006; updated version Aumont et al., 2015). ~~Although more recent versions were available at production, this model version was used to be consistent with configuration development, starting with~~

Although NEMO version 3.6 was available at the time of production, version 3.4 was retained for consistency with the configuration development workflow, which involved a hierarchy of tests ~~of increasing resolution on which model parameterswere tested. This model run was configured from two other previous model runs from the DRAKKAR Group and will be referred to several times below~~across increasing resolutions used to evaluate model parameters. BIOPERIANT12 was configured building on two prior model runs developed by the DRAKKAR group: ORCA12-MAL101, a global~~physics only run (Barnier et al., 2014; Lecointre~~ , eddying physical configuration (Barnier et al., 2014; Lecointre et al., 2011), and BIOPERIANT05-GAA95b, an eddy-permitting ~~SO configuration including biogeochemistry~~ 1/2° SO biogeochemical configuration (Albert, A., pers. comm~~, MEOM-DRAKKAR group), an updated model of Dufour et al. (2013) from which we derived our designation of~~ ., MEOM–DRAKKAR Group), itself an update of the model described in Dufour et al. (2013), from which the BIOPERIANT12 designation was derived.

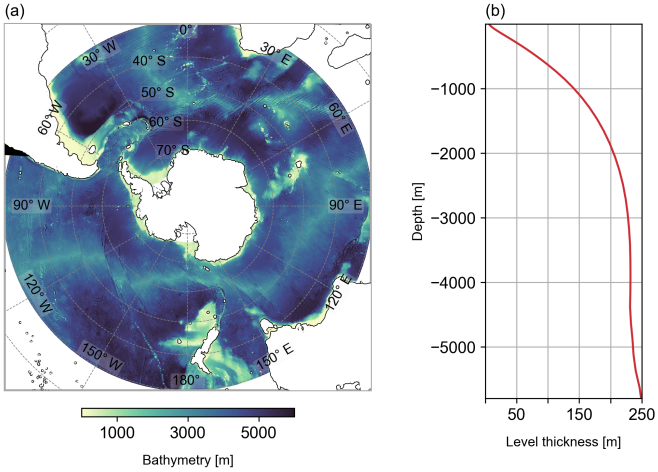

Figure 1. BIOPERIANT12 grid configuration **(a)** domain showing model bathymetry and **(b)** vertical grid cell thickness ~~versus~~ as a function of depth.

2.1 Domain and grid

The model grid and bathymetry for the ~~Southern Ocean~~ SO south of 30° S (Fig. 1a) is a subset of the global tripolar ORCA12 grid with 46 vertical levels built from the ETOPO2 dataset combined with the GEBCO one minute grid. The horizontal grid, at 1/12° resolution (∼8 km at 30° S, 4.6 km at 60° S), can be considered eddy-resolving. The vertical grid of BIOPERIANT12 consists of 46 z-coordinate levels with partial bottom steps. For the surface ocean mixed layer fluxes and biogeochemistry, there are 15/18 levels in the upper 200/400 m, with vertical resolution ranging from 6–40 m. Below this, grid thickness increases: ∼200 m at 2000 m depth (z = 29) and finally 250 m at the bottom (Fig. 1b).

2.2 Initial conditions

To obtain a representative and stable surface ocean state, BIOPERIANT12 is initialised from rest~~and for tracers from respective climatological products~~, with temperature, salinity and biogeochemical tracers derived from climatological data products. This model thus starts from a contemporary ocean state with large-scale climatological gradients and minimises spin-up. For the ocean, ~~Levitus~~ the initial temperature and salinity ~~climatology (Locarnini et al., 2010) were used~~fields are taken from the World Ocean Atlas (WOA) Levitus January climatology (Locarnini et al., 2010). Sea ice ~~initial conditions are from the~~ is initialised using January ice climatology ~~for~~ averaged over 1998–2007 from the ORCA12-MAL101 simulation, when sea ice ~~is at a minimum in the seasonal cycle and thereafter freely evolves with the~~ extent is low. Thereafter, sea ice evolves freely under the dynamics of the LIM2 model~~. Biogeochemical tracers were~~ , responding to the simulated thermodynamic and dynamic forcing.

Biogeochemical tracers are initialised from coarse-resolution ~~climatologies: dissolved~~ observational climatologies which provide realistic large-scale distributions. Dissolved inorganic carbon (DIC), total alkalinity (TA) are obtained from the GLODAP annual mean climatology (Key et al., 2004); while nutrients including nitrate (NO_3), phosphate (PO_4), silicate (Si) and oxygen (O_2) are taken from the January monthly ~~WOA09 climatology (Garcia et al., 2013, 2010); dissolved~~ climatology of WOA09 (Garcia et al., 2013, 2010). Dissolved organic carbon and iron ~~were consistent with~~ fields are inherited from the BIOPERIANT05-GAA95b ~~initialisation 90 from an ORCA05 run. The other tracers were initialised with constant values set in PISCES~~simulation due to lack of climatological dataset and particularly the importance of iron to the region. BIOPERIANT05-GAA95b was initialised with the same biogeochemical tracers as above and with remaining tracers from global model initial conditions (ORCA2, NEMO Consortium, 2020). Its output provides an internally consistent distribution of the aforementioned fields for the SO and is thus also used for boundary conditions. The remaining tracers in PISCES are initialised with uniform values as per standard model defaults.

2.3 Boundary Conditions

BIOPERIANT12 has one open lateral boundary ~~in~~ to the north. ~~Boundary~~ Interannually varying boundary conditions for the dynamics were ~~derived from an ORCA12–MAL101 from the~~ obtained from the global 1/12° ORCA12-MAL101 simulation, using available 5 day averages for the period 1989–2009. While ~~the BIOPERIANT12 dynamical open~~ these physical boundary conditions are ~~of a comparative 1/12resolution,~~ at a comparable resolution, suitable high-resolution biogeochemical boundary conditions were not available at ~~this high resolution at~~ the time of ~~preprocessing; we therefore obtained them~~ setup. Therefore, biogeochemical fields were taken from the coarser 1/2° BIOPERIANT05-GAA95b ~~. A~~ simulation. Rather than using the full interannual series, which in coarse-resolution models can result in biases in the seasonal and vertical structure of DIC, and hence in the simulated seasonal cycle of carbon (Mongwe et al., 2016), a climatological "normal year" boundary forcing ~~consisting~~ was constructed. This consisted of 5 day ~~averages for~~ averaged fields computed over the period 1995–2009~~was calculated and used as opposed to the interannual dataset due to reported biases in certain biogeochemical tracers (Mongwe et al., 2016). For the lateral boundary of the coastlines partial free slip is prescribed~~.

At lateral solid boundaries, partial free-slip conditions are applied. Surface atmospheric forcing ~~data are from ERA-interim (Dee et al., 2011)using~~ is provided by ERA-Interim reanalysis data (Dee et al., 2011), applied through the CORE bulk ~~formulation. Wind components are supplied at 3 hourly~~ formulae. Wind stress components are prescribed at 3-hourly intervals using the absolute wind formulation~~thus neglecting effects of~~ , which does not account for the surface ocean current ~~on the wind~~ effect on wind speed. Sea surface ~~restoring of salinity~~ salinity is weakly restored to monthly Levitus climatology values. Additionally, a restoring term is applied to ~~Levitus monthly climatology is applied. Restoring for~~ Antarctic Bottom Water ~~is applied to counteract the drift in ACC transport due to the representation of deep waters~~ to counteract a known drift in Antarctic Circumpolar Current (ACC) transport from deep water structure in the DRAKKAR models (Dufour et al., 2012).

2.4 Model evolution

The model is ~~run for the duration~~ integrated over the 21 year period from 1989 to 2009, the same period for which the ORCA12 boundary conditions were available. ~~The model integration was carried out with a~~ A baroclinic time step of 360 ~~s. Within the first 5 years of initialisation~~ seconds is used. During the first five years of integration (1989–1994), the surface ocean dynamics ~~reach statistical equilibriumand~~ adjust to the imposed forcing and initial conditions, reaching a statistical equilibrium. Key indicators such as transport through the Drake Passage ~~stabilises, years 1989 to 1994 are therefore designated as spin-up~~ also stabilise during this period (Fig. S1, S2)~~. Thereafter the model is run to 2009 with output saved as~~ , and thus these years are designated as the spin-up phase. From 1995 onward, the simulation proceeds under quasi-equilibrated conditions, with 5 day ~~averages and the final 10 years~~ averaged output saved for analysis. The final decade of the simulation (2000–2009) ~~were analysed. At depths below~~ is used for evaluation.

While the focus of the configuration is on upper ocean processes, particularly in the top 1000 m, it is noted that a gradual drift in deep ocean temperature (below 400 ~~*m*, temperature shows a significant drift from~~ m) becomes apparent from around 2002 ~~, while the aim is to simulate surface ocean processes, this must be noted~~ onward (Fig. S1e–g). This drift does not impact the surface dynamics or the primary objectives of the study, but should be considered when using the model output for investigations involving deep ocean processes.

2.5 Model Numerics

~~Ocean~~ Advection of ocean tracers (temperature and salinity) ~~advection~~ is implemented with the TVD scheme, while passive biogeochemical tracers in PISCES tracers are advected using the MUSCL advection scheme. Lateral diffusion ~~of both ocean and passive tracers is achieved with~~ for both physical and biogeochemical tracers is applied via a laplacian operator along isonetural surfaces. Lateral advection of momentum uses a leapfrog scheme~~; momentum diffusion uses the~~ , and momentum diffusion implemented using a bilaplacian operator along geopotential surfaces. ~~Vertical mixing in the model uses the~~

Vertical mixing is represented using the turbulent kinetic energy (TKE) closure scheme. For background subgrid-scale mixing~~in the background~~, vertical eddy viscosity and diffusivity coefficients are set to 1.2 x 10^{-4} m^2 s^{-1} and 1.2 x 10^{-5} m^2 s^{-1} from default configuration namelists, e.g. ORCA2 (NEMO Consortium, 2020). At the ~~bottom~~ocean floor, a diffusive bottom boundary layer scheme is ~~used as well as the advective bottom boundary layer scheme for the case~~ employed along with an advective scheme to account for downslope transport in cases of dense water overlying ~~less dense water at the bottom~~ lighter water masses (Gurvan et al., 2019). The bottom boundary is set with a nonlinear bottom friction formulation.

2.6 Computational Requirements

Development of BIOPERIANT12 ~~started after the introduction~~ began following the deployment of the Lengau ~~cluster of NICIS-CHPC (~~high-performance computing (HPC) cluster at the National Integrated Cyberinfrastructure System's Centre for High Performance Computing (NICIS–CHPC) in late ~~2016, which comprises of~~ 2016. Lengau, a shared resource for the South African research community, comprises approximately 32 832 Intel ~~XEON~~ Xeon CPU cores when fully operational~~and is a~~

shared HPC resource of the South African research community. The final iteration, this reference simulation , was run reference simulation presented in this study was completed in 2020. Due to South African electricity restrictions, constraints related to national electricity which reduced available compute capacity, resource allocation and system stabilitydecrease, to compensate for this, we chose to use more storage space to create and save restart files more frequently. Even with the NEMO system stability, and resource allocations, model runs required operational adjustments. To mitigate risks of unexpected interruptions and ensure continuity of simulations, restart files were written more frequently at the expense of increased storage usage.

After applying NEMO's land elimination algorithmeliminating , which excluded 19 % of the non-ocean subdomains subdomains with no active ocean points, the simulation was run using 3,3240 CPUswere chosen to balance model scaling and wall clock timefor running and saving 240 CPUs. This configuration optimised the trade-off between model scalability and wall-clock time, while efficiently managing the regular output of ocean, iceand BGC , and biogeochemical fields at 5 day outputs intervals, as well as the frequent writing of restart files.

3 Model Evaluation

We evaluate BIOPERIANT12 the physical and biogeochemical fields of BIOPERIANT12 by comparing key metrics of the upper-ocean for the last upper-ocean metrics from the final 10 years of the experiment , (2000–2009, against observations) against observational data (OBS), for which temporal and spatial coverage improves within during the 2000s. Observational datasets are provided cited inline and summarised in Table 1. We note that many Many of these datasets are low resolution-resolution, gridded products, which is only applicable in are primarily applicable for evaluating the large-scale mean-state. We check mean state.

As an initial comparison, we verify that the model reproduces the annual and seasonal mean statesas an initial comparison and then follow this with , followed by an assessment of the characteristics of temporal variability. In Section 3.1, we evaluate the model's physical ocean and sea ice properties as an indication indicators of model stability and the general circulationaffecting general circulation, which in turn influence the BGC tracers,. This evaluation is guided by the metrics proposed by Russell et al. (2018) for the evaluation of the assessing the SO in coupled climate models and ESMs.

As a summary , preceding further evaluation of the BGC outputand precursor to further BGC evaluation, we present biomes and summarisw the model output compared to that of observations (Section 3.2)biome classifications and summarise model output in comparison to observations in Section 3.2. In Section 3.3, we present modelled carbon. Finally, focus on modelled carbon, while Section 3.4 provides further analysis of biogeochemical and biological propertiesare further analysed in Section 3.4.

BIOPERIANT12 Drake Passage transport vs selected estimates from literature Transport SvSource Reference 145.25 5.66 BIOPERIANT12 134 11.2 Observations Whitworth and Peterson (1985) 173.3 10.7 Observations after 2007 Donohue et al. (2016) 149.2 Model 0.5resolution (PERIANT05) Dufour et al. (2012) 143.2 Model 0.25resolution (PERIANT025) Dufour et al. (2012) 155 51 CMIP5 multi-model mean (1resolution) Meijers (2014) 134–173 OMIP–2 models eddy-resolving Chassignet et al. (2020)

Table 1. Summary of observational datasets used for model evaluation

Variable	Temporal resolution and coverage	Horizontal resolution	Dataset and reference URL
Currents u, v	2000–2009	0.25°	AVISO altimetry (The Ssalto/Duacs altimeter products were produced and distributed by the Copernicus Marine and Environment Monitoring Service, CMEMS, http://www.marine.copernicus.eu)
Temperature, Salinity	Monthly climatology	0.25°	WOA2013 (Locarnini et al., 2010)
Polar Front position	Weekly 2002–2009	0.25°	Satellite AMSR-E, AMSR-2, WindSat (Freeman and Lovenduski, 2016)
MLD gridded	Monthly climatology	1°	Argo profiles (Holte et al., 2017)
T/S profiles	2002–2009		Argo profiles (Holte et al., 2017)
Sea ice concentration	2000–2009	0.25°	NOAA/NSIDC (Meier et al., 2017; Peng et al., 2013)
Mean biomes	Mean over 1998–2010	1°	Biome dataset (Fay and McKinley, 2014)
FCO_2, pCO_2	Monthly means	1°	CSIR-ML6 multi-platform machine-learning product (Gregor et al., 2019)
DIC, TA	Annual mean centred 2002	1°	GLODAPv2 (Olsen et al., 2016; Lauvset et al., 2016)
Dissolved iron	Binned into months	1° bins	Dissolved iron in situ profiles (Tagliabue et al., 2014)
NO_3, PO_4, Si	Monthly climatology	1°	WOA13 (Garcia et al., 2010)
Dissolved oxygen	Monthly climatology	1°	WOA13 (Garcia et al., 2013)
Chloropyll-a	Weekly 2000–2009	9 km	OC-CCI-v6 mixed satellite in situ chlorophyll-a (Sathyendranath et al., 2019)

3.1 Key physical ocean metrics in the Southern Ocean

3.1.1 Transport through Drake Passage

Transport of the ACC through the Drake Passage ~~at~~ was calculated by integrating the model's zonal velocity from surface to bottom across 69° W~~in~~. The time evolution of transport (Fig. S1b), shows that BIOPERIANT12 is stable after spin-up~~(Fig. S2), with~~, with an annual mean transport through the Drake Passage from 2000–2009 at 145.25 ± 5.66 Sv. ~~The~~ This value is comparable ~~with observations~~ to observational estimates, as summarised in Table 2, such as the ~~generally accepted~~

Table 2. Drake Passage volume transport in BIOPERIANT12 compared with selected estimates from the literature

Transport [Sv]	Source	Reference
145.25 ±5.66	BIOPERIANT12	
134 ±11.2	Observations	Whitworth and Peterson (1985)
173.3 ±10.7	Observations after 2007	Donohue et al. (2016)
149.2	Model 0.5° resolution (PERIANT05)	Dufour et al. (2012)
143.2	Model 0.25° resolution (PERIANT025)	Dufour et al. (2012)
155 ±51	CMIP5 multi-model mean (1° resolution)	Meijers (2014)
134–173	OMIP-2 models eddy-resolving	Chassignet et al. (2020)

~~observational~~ widely accepted estimate of 134 ± 11.2 Sv by Whitworth and Peterson (1985)~~; although~~. However, post-2007 estimates of transport ~~taken after 2007 yield values higherthan this, e.g~~ are higher, such as 173.3 ± 10.7 Sv (Donohue et al., 2016) ~~, attributed to higher resolution observations and~~ which is attributed to the increase of resolution in observations. This higher value is used as the observational benchmark ~~for the model analysis of~~ in model intercomparisons from CMIP3 to CMIP6 ~~models by Beadling et al. (2020). It~~ (Beadling et al., 2020). The mean transport of BIOPERIANT12 also compares well to its similar SO regional model ~~"predecessors"~~ predecessors, PERIANT05 and PERIANT025 ~~of~~ (0.5° and 0.25° resolution, respectively), with respective mean transports of 149.2 Sv and 143.2 Sv (Dufour et al., 2012)~~, as well as~~. Additionally, it aligns with estimates from global models such as the multi-model mean of 155 ± 51 Sv for CMIP5 ~~global~~ models of mostly 1° resolution (Meijers, 2014) and ~~similar to~~ the eddy-resolving Ocean Model Intercomparison Project phase 2 (OMIP-2) models ~~that~~ which fall within the chosen observation range of 134–173 Sv (Chassignet et al., 2020).

3.1.2 Eddy Kinetic Energy (EKE)

~~Figure 2 shows the~~ The climatological annual mean surface EKE for 2000–2009 ~~for the model compared to the EKE derived from~~ in BIOPERIANT12, compared to that derived from the AVISO 1/4° gridded altimetry dataset~~. The~~, is shown in Fig. 2. The spatial distribution of EKE in the model is in general agreement with observations, ~~regions of high EKE such as those~~ capturing elevated EKE in regions associated with western boundary currents (WBC) and downstream of ~~topography are represented in the model~~major topographic features. Zonally averaged EKE bands are comparable to SO models by Munday et al. (2021, Fig. 7a), although BIOPERIANT12 shows slightly higher EKE than their models, except for the WBC regions. ~~BIOPERIANT12 appears to overestimate EKE except~~ For example, in the Agulhas Current region (Fig. S3), EKE is underestimated compared to observations, reflected as the lower zonal mean EKE between 36 and 43° S (Fig. 2a)~~particularly from the Agulhas Current region (Fig. S2) as seen in the meridionally averaged EKE between~~, possibly from missing dynamics around the Agulhas Retroflection region (15–45° E~~(Fig. S3~~; Fig. S2b). Models at similar resolutions are able to represent the distribution patterns of EKE ~~(e.g. ORCA12, (Rieck et al., 2015; Patara et al., 2016)),~~ (e.g. ORCA12, Rieck et al., 2015; Patara et al., 2016), although magnitudes may differ. ~~Most~~

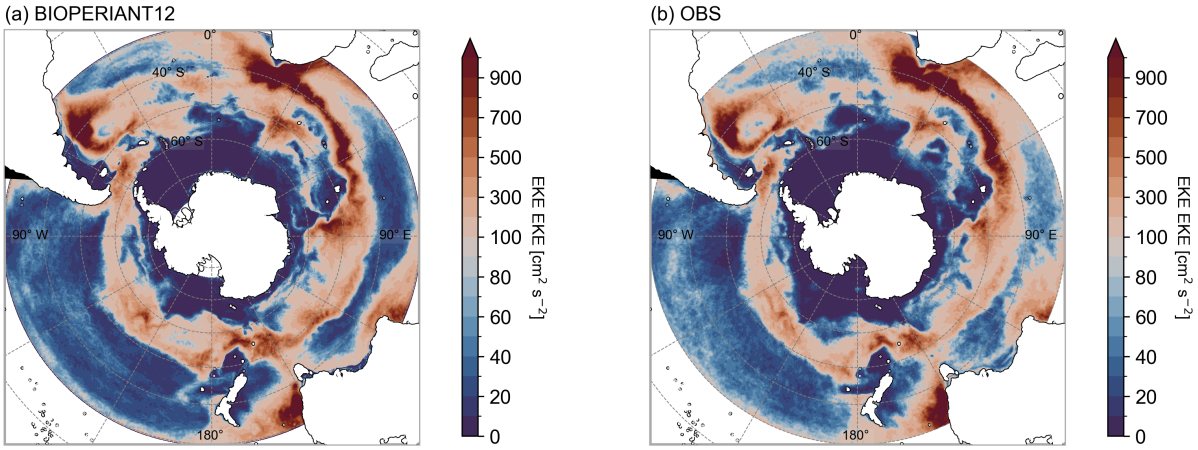

Figure 2. Annual mean surface EKE for years 2000–2009 ~~for~~ from **(a)** BIOPERIANT12 ~~model~~ and **(b)** the AVISO 1/4° dataset.

OMIP-2 ocean models (at ∼1/10°) ~~underestimate EKE with some contribution from~~ generally underestimate surface EKE, partially due to factors such as temporal averaging (Chassignet et al., 2020)~~, regional effectsmay also contribute~~; regional effects: high EKE regions are eddy-rich but ~~their spatial coverage~~ exhibit reduced spatial extent in OMIP-2 models ~~are smaller than observations(AVISO)~~ compared to observations, while eddy-poor regions ~~have greater spatial coverage. Regional~~ tend have greater coverage. In contrast, the regional model MOMSO (Dietze et al., 2020) ~~, on the other hand,~~ overestimates EKE, which is attributed to the ~~higher model than observational dataset resolution, degrading modelspatial resolution obtains more comparable magnitudes . With consideration to~~ lower resolution of the observational dataset used for comparison. However, when the model's spatial resolution was degraded to match that of the dataset, comparable magnitudes were obtained. Considering factors such as regional differences, ~~such as in~~ the effect of winds (Patara et al., 2016)~~and applying the~~ , and the use of the absolute wind formula which neglects the effect of current-wind interactions ~~and~~ which reduces eddy energy (Renault et al., 2016; Munday et al., 2021), BIOPERIANT12 ~~EKE describes a surface SO with reasonable mesoscale eddy representation with which physical dynamics towards model improvement and BGC questions can be addressed~~provides a reasonable representation of mesoscale surface variability in the SO, supporting its use in exploring physical–biogeochemical interactions and addressing key BGC research questions.

3.1.3 Frontal structure

The SO fronts help describe the larger ACC structure, ~~with their~~ characterised by steep horizontal gradients and associated strong vertical ~~motion, they demarcate regions of consistent water~~ motions, these fronts delineate regions with consistent water mass and nutrient properties, as well as regions of air–sea CO_2 in- and out-gassing~~:~~ , specifically CO_2 in-gassing north of the Polar Front (PF) and out-gassing between the PF ~~southwards to~~ and the marginal ice zone (Mongwe et al., 2018). Latitudinal

variations in the frontal positions will thus reflect as shifts in the positions of these fronts can lead to local changes which affect heat and carbon fluxes and are therefore thus used as a SO model evaluation metric by Russell et al. (2018), the .

The positions of the SubAntarctic Front (SAF) and PF are chosen out of all the SO fronts, as representing the to represent the northern boundary and the central ACC, respectively. Their method uses Following Russell et al. (2018), we apply a simplified subsurface temperature criteria criterion, consistent with (Orsi et al., 1995)which allows easy inter-model and model-observation comparisons, to identify these fronts: the SAF is defined by the 4 °C isotherm at 400 m and the PF by the 2 °C isotherm in the upper 200 m. In Figure This approach allows easy inter-model and model–observation comparisons.

In Fig. 3, we present the annual-mean annual mean position and standard deviation of the SAF and PF for in BIOPERIANT12 interannual monthly-means, compared to those calculated from monthly means for the 2000–2009 period. These are compared to fronts derived from WOA13 temperature (climatological months)monthly temperature climatology, the satellite-derived PF of Freeman and Lovenduski (2016), and Orsi et al. (1995)the Orsi et al. (1995) dataset, as used by Russell et al. (2018). In general, spatial meridional variabilities in the model frontal positions are Overall, model fronts show spatial meridional variability consistent with the observation-derived fronts, but with a south southward bias by up to 3° in latitude, showing . This is accompanied by "pinching" of the fronts from topography such as in regions of strong topographic influence, such as the Drake Passage, Campbell Plateau (170° E) and the Southwest (30° E) and Southeast (80° E) Indian Ridge, followed by diverging of the SAF and PF downstream. However, the difference in the model PF in

A notable discrepancy is observed in the modelled PF within the Indian Ocean stands out, highlighting the nature of averaging or the temporal under sampling of datasector, which may reflect the effects of temporal averaging or limited sampling of the observational datasets. At the Kerguelen Plateau (∼75° E), the model follows either the PF follows either a northern or southern branch but the mean PF reflects the southern path (see path but the temporal mean simulated PF is highly variable in latitude (standard deviation) aligning with the southern branch (Fig. S4)accompanied by very high standard deviation in contrast to . This contrasts with the observational data that show the mean path favours the northern branch over the northern plateau (Dong et al., 2006; Wang et al., 2016). As with the Similar to examples provided by Russell et al. (2018), the chosen models models evaluated (CMIP5 models at ∼100 km) do not completely or consistently capture similar patterns to the observations, reflecting their individual model model-specific biases as well as their coarser resolution(CMIP5 models at ∼100 km). limitations of coarse resolution.

As shown in model EKE in Fig. 2, the mean mesoscale dynamics of the SO are captured by BIOPERIANT12, this includes the complex frontal dynamics described in observational studies BIOPERIANT12 captures key aspects of SO mesoscale dynamics, including complex frontal behaviours such as branching, jets and front-eddy interaction (Freeman and Lovenduski, 2016; Chapm which ultimately affects the calculated frontal positions particularly, a temperature-derived definitionjet structures, and front–eddy interactions observed in satellite and in situ data (Freeman and Lovenduski, 2016; Chapman, 2017). Since frontal positions used a temperature-based criterion, they are sensitive to the representation of such mesoscale features. The high variability in frontal dynamics of the mesoscale-resolving positioning driven by eddies in BIOPERIANT12 , leads to model-observation differences, especially for regionscan lead to inconsistencies with observations, particularly in regions, such as the Kerguelen Plateauwhich is dominated by eddies as opposed to the meandering of the core jets (Shao et al., 2015); additionally, we expect

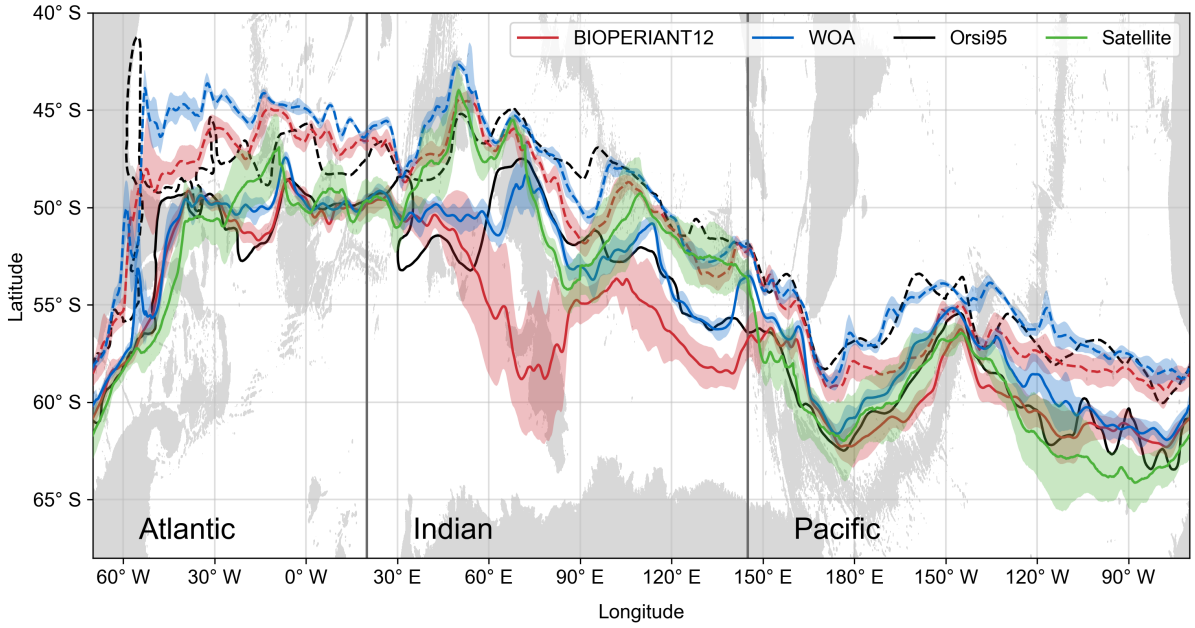

Figure 3. Annual mean latitudinal position of the SubAntarctic Front (dashed line) and Polar Front (solid line) derived from temperature in BIOPERIANT12 (2000–2009)~~compared to~~ , WOA13, the dataset of Orsi et al. (1995), and satellite SST Polar Front (2002–2009) from Freeman and Lovenduski (2016)~~and Orsi et al. (1995)~~. Colour shaded regions are the standard deviation of the front using ~~monthly-mean~~ monthly mean temperatures. Grey shaded regions ~~indicate the land mask and~~ show bathymetry shallower than 3000 m~~(lighter grey)~~.

~~a corresponding improved~~ , where frontal locations are more strongly influenced by eddy activity than by the more stable meandering of coherent jets (Shao et al., 2015). Nonetheless, the model's improved representation of mesoscale processes is expected to support more realistic exchange of water masses and biogeochemical properties (Rosso et al., 2020). ~~This complicates this metric for model-observation comparison but frontal position is still useful to delineate model~~ While this complexity complicates direct model–observation comparison of frontal positions. The use of fronts remains valuable for delineating regions for analysis.

3.1.4 Mixed Layer Depth

To evaluate the MLD ~~of~~ in BIOPERIANT12, we ~~chose~~ use in situ measurements given by the Argo floats database as our observational reference (Table 1). MLD ~~from both sources were~~ for both the model and observations was calculated from temperature and salinity ~~values and using~~ profiles following the de Boyer Montégut et al. (2004) density threshold of 0.03 kg m^{-3} ~~from~~ relative to a reference depth of 10 m, a method that has been shown to be robust for ~~Southern Ocean~~ SO profiles (Dong et al., 2008; Treguier et al., 2023). ~~While the Argo platform presents~~ Although Argo float coverage has spatial and temporal gaps ~~in their coverage~~ (Fig. S5), the temperature and salinity profiles collected by the floats ~~ultimately captures the~~ provide direct measurements that capture real-world variability and mixing features, ~~in opposition to~~ unlike reanalysis products

which ~~introduce an unknown source of uncertainty depending on their reanalysis model. Model MLD was then~~ may introduce additional uncertainties due to model-dependent biases.

To ensure a consistent comparison, model MLDs were sampled according to the Argo observational coverage. ~~MLD observations were binned into~~ Observed MLDs were binned onto a 1° x 1° regular grid and averaged ~~to monthly intervals across~~ into monthly intervals over the period 2001–2009. ~~This was also done for model MLD~~ The same gridding and temporal averaging was applied to the model output, which was then ~~further~~ subsampled to the same locations and months as Argo observations. The ~~seasonal-spatial~~ resulting seasonal–spatial patterns and amplitude in MLD are shown in Fig. 4.

Overall, the spatial distribution of ~~the observational and~~ BIOPERIANT12 MLDs ~~agree well , for~~ compares well with observations during both the minimum ~~and maximum MLD months, January and September, respectively~~ (January) and maximum (September) MLD months (Fig. 4a–b, d–e). ~~A comparison of the magnitudeof the summer MLD (Fig. 4c) shows~~ However, in terms of magnitude, simulated summer MLDs within the ACC ~~, the BIOPERIANT12 MLD is~~ are too deep by ~~around~~ ∼50 m~~while it is too shallow by around 50 m in the~~ , while MLDs north of the SAF ~~. For winterMLDs~~are too shallow by a similar amount (Fig. 4c). In winter, BIOPERIANT12 generates deeper MLDs relative to ~~the observational estimates (by about~~ observations, with a bias of ∼100 m ~~; Fig. 4f)~~ in the Pacific sector of the SO ~~. Despite the magnitude difference, BIOPERIANT12 captures the deep winter MLDs (exceeding~~ (Fig. 4f). Despite this bias, the model correctly captures the pattern of deep winter mixed layers (> 400 m) ~~confined to~~ in the Pacific and Indian sectors~~showing that the model is responding~~ , indicating that it responds appropriately to atmospheric forcing and ~~forming deep waters~~ forms deep water masses in the expected regions. ~~An important component~~

The seasonal evolution of the MLD is a key diagnostic in the SO ~~is the seasonal cycle~~ (Fig. 4g). The model reproduces the observed cycle of winter deepening and summer shoaling~~of the simulated MLD agrees well with the seasonal cycle of the observations~~, with a ~~monthly climatology Pearson correlation of r~~ Pearson correlation coefficient of R = 0.97 for monthly climatologies. The shallow ~~limit of the simulated climatological MLD follows the observations well during DJFM, however the deep MLD limit departs from the observations~~ seasonal limit of simulated MLD aligns closely with observations during DJFM. However, the model departs from observed values around April, ~~where~~ with standard deviations of the monthly mean MLDs ~~show~~ showing the BIOPERIANT12 ~~MLD extending to~~ mixed layer extending over 100 m deeper than observations in September (MLD maximum)~~than what the observations show~~. Treguier et al. (2023) showed that in OMIP models, even with horizontal resolutions ranging from 1° down to 1/16°~~horizontal resolution, MLD is hard to constrainand increasing model resolution to include the mesoscale does not consistently improve MLD depth~~ , MLD remains difficult to constrain, and higher resolution does not always result in improved representation of MLD in the SO. Nevertheless, despite its winter deep bias, the seasonal cycle and variability of ~~the~~ BIOPERIANT12 MLD ~~agrees well with the observations, despite over-deepening during winter~~compares favourably with observations.

3.1.5 Ocean Heat Content (OHC) and Temperature

~~BIOPERIANT12 temperature and OHC for the upper 400 m appear to compare well~~ Large-scale climatological temperature and 0–400m OHC in ~~seasonal~~ BIOPERIANT12 compare well with observations in terms of spatial distribution (Fig. S6).

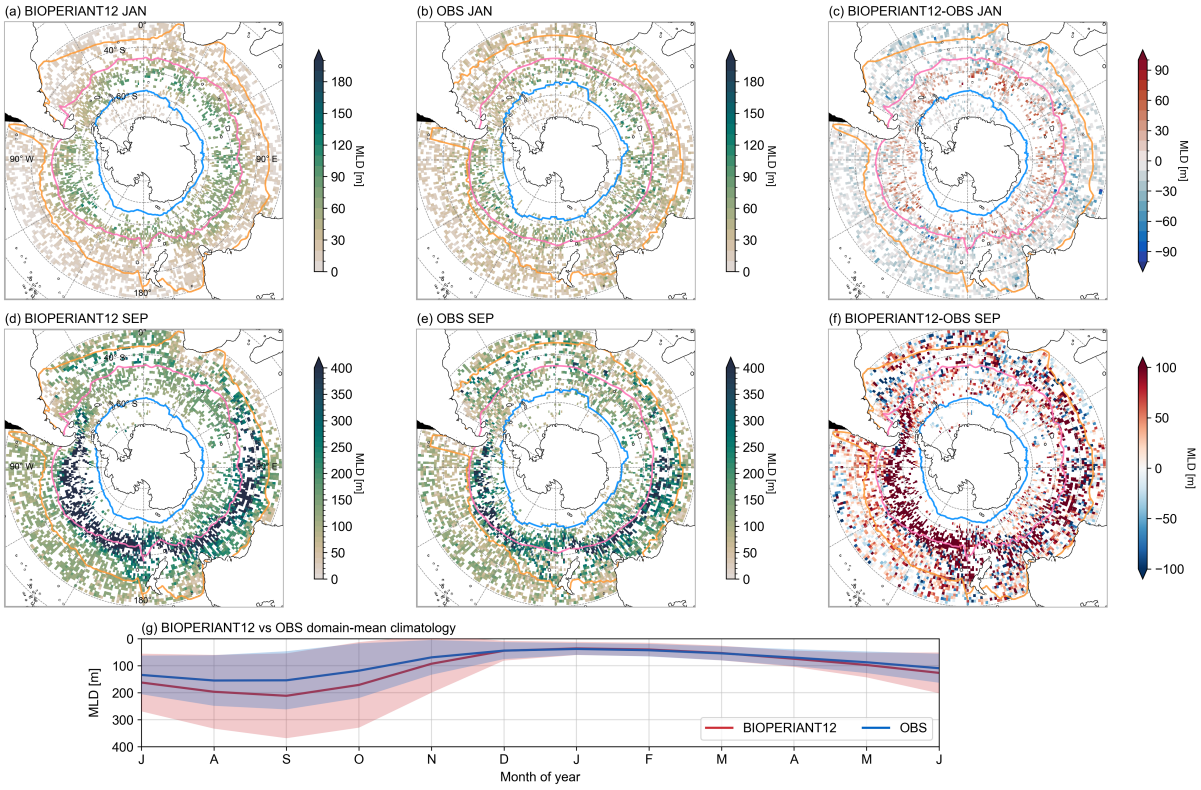

Figure 4. Seasonal comparisons of MLD from **(a, d)** BIOPERIANT12, averaged monthly and co-located to monthly averaged Argo MLDs ~~in~~ on a $1° \times 1°$ regular grid, **(b, e)** Argo float observations, and **(c, f)** model–observation difference, for January and September climatologies, respectively. Maps are overlaid with the northern ~~climatological~~ mean biome borders corresponding to model/data SO biomes. **(g)** Climatological seasonal cycle of monthly MLD, domain-averaged over the entire SO.

~~While no surface temperature correction has been applied to the model, it is relatively stable over the last 10 years of the~~ ~~model but model–data climatological differences between BIOPERIANT12 and WOA13 temperature and OHC show spatial~~ ~~variations in the mesoscale model fields~~ A spatial map of model–observation differences reveals variability that appears linked to mesoscale activity (Fig. ~~S7a, c). OHC in the model has a warm bias (domain mean around~~ S7a–d), particularly given the coarser resolution of the WOA13 dataset (1/4°). In terms of magnitude, the model shows a higher domain mean 0–400 m OHC (~13 x 10^9 J m^{-2}, Fig. S7e) ~~, although SST shows~~ compared to observations, despite exhibiting a cool bias ~~(Fig. S7b, d). While SO surface temperatures in models generally show warm biases (Beadling et al., 2020) and the opposite is shown for BIOPERIANT12 SST (Fig. 7f, domain-mean SST solid line), the deeper, domain-mean~~ in sea surface temperature (SST) as shown in Fig. S7(b, d, f). This discrepancy can be attributed to a warm bias in subsurface temperatures at 200 m and 400 m ~~are warmer than observations~~ (Fig. ~~S7f, dotted, and dashed lines)despite the low resolution, area-weighting of the dataset.~~

~~The model–data differences are consistent over the run duration, the model is initialised with climatology and after~~ S7g). This result contrasts with the commonly observed warm SST bias in many SO models (Beadling et al., 2020).

Following initialisation with climatological fields and spin-up~~shows~~ , upper ocean temperatures in the model (upper 200 m) exhibit no significant drift over the simulation period (Fig. ~~S7g), the resultant stable upper ocean structure over the model analysis period suggests that the dynamics are also stable , possibly from increased mesoscale dynamics of the model which also influenced frontal definition above. Thus, we disregard the creation and influence of spurious features in the simulation that may propagate while altering the physical and biogeochemical fluxes, and any biogeochemical biases can be considered systematic or from model~~ S1c–d), even without the use of surface temperature restoring. Combined with the stable surface EKE discussed earlier, this suggests that surface ocean dynamics in BIOPERIANT12 remain stable throughout the analysis period. Given the consistency of model–observation biases, we do not attribute discrepancies in the physical or biogeochemical fields to spurious or transient model behaviour. Rather, remaining biases likely reflect systematic differences tied to consistent model behaviour or specific model design choices.

3.1.6 Sea ice

Sea ice plays ~~an important~~ a key role in setting the seasonal freshwater flux in the SO. ~~Melting~~ Seasonal melting in the spring/summer and growth in autumn/winter ~~sets the surface ocean salinity and thus has direct consequences for~~ strongly influence surface salinity and thereby affect both vertical and horizontal stratification dynamics (Giddy et al., 2021, 2023) ~~and~~ as well as large-scale water mass transformation (Abernathey et al., 2016). For ~~the model comparison, National Sea Ice Data Centre~~ comparison with the model, observational mean monthly sea ice concentration data from the National Snow and Ice Data Center (NSIDC) ~~sea ice observations mean monthly data~~ for the period 2000–2009 were used (Table 1). Data ~~shows~~ show sea ice grows northward from the Antarctic continent ~~in~~ during the winter months, ~~peaking with~~ reaching maximum extent in September and then melts, retreating southwards, towards the Antarctic continent ~~to reach~~ reaching a minimum ice extent in February (Fig. 5).

The spatial comparison ~~for~~ of minimum/maximum ~~climatological months~~ sea ice extent (Fig. 5a, b) shows ~~model maximum extent is comparable spatially to data~~ that the model reproduces the spatial pattern of winter maximum reasonably well but overestimates the ~~sea ice growth by~~ total extent by about 1–2 million km^2, around 10 % of the ~~winter sea ice~~ observed winter maximum (Fig. 5c, d). ~~Data shows minimum sea ice extent~~ Observations indicate a minimum in February, ~~while in the model minimum occurs over~~ whereas the model shows similar minimum values spanning February and March~~with similar values~~. The timing of sea ice ~~growth and melt by~~ advance and retreat in BIOPERIANT12 ~~relative to the observations (Fig. 5c, d) indicates that the model responds well to~~ suggests a realistic response to seasonal heat fluxes~~with minimum and maximumextent agreeing with the observations, particularly in the winter. Although the~~ , with good agreement during winter maximum. However, the model does not melt ~~sufficiently~~ enough ice in December (∼2 million km^2 ~~relative~~ compared to∼5 million km^2 ~~from the observation) , it compensates for this by not melting the remainder of the necessary sea ice in~~ in observations) and compensates by continuing to melt through February (∼5 million km^2 ~~relative to~~ in the model vs. ∼2 million km^2 ~~from~~ in the observa-

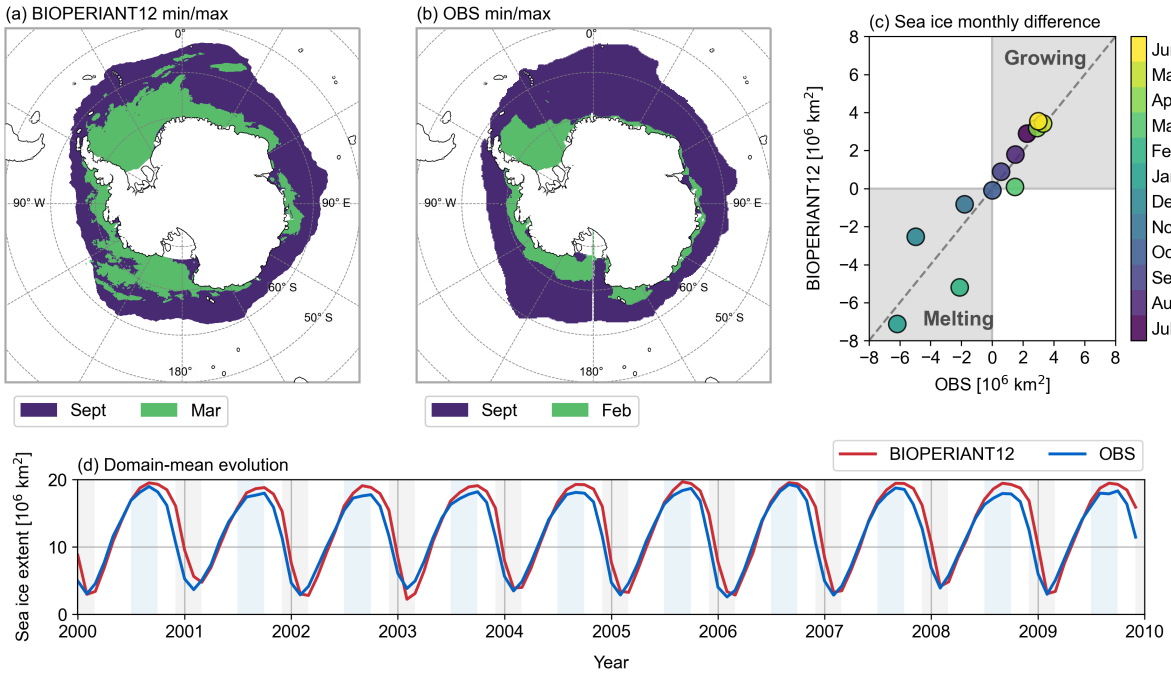

Figure 5. ~~Climatological-mean~~ Climatological mean sea ice extent ~~of~~ for the maximum (blue) and minimum (green) months for **(a)** BIOPERIANT12 and **(b)** NSIDC observations. **(c)** Climatological ~~monthly-mean~~ monthly mean sea ice extent difference indicating growth and melt for the BIOPERIANT12 simulation vs. NSIDC observations. **(d)** ~~Timeseries~~ Time series of ~~monthly-mean~~ monthly mean sea ice extent from the BIOPERIANT12 model (red) and NSIDC observations (blue).

tions)~~before both the~~ , before both model and observations ~~show sea~~ begin to show ice growth from March onwards (Fig. 5d; S8b). ~~Overall, the sea ice in~~

Overall, BIOPERIANT12 ~~provides a stable temporal view of the seasonal cycle , with more interannual variability seen in the summer~~ captures a stable seasonal cycle in sea ice, with the largest interannual variability occurring during the summer months (Fig. S8b).

3.2 Biomes

3.2.1 Biome definition

To evaluate the biogeochemical and carbon fields, we ~~chose to use~~ apply the biome classification method ~~(Fay and McKinley, 2014) , over static geographic definitions or that from ocean physics (e.g. by fronts, a dynamical field), thus combining both large scale~~ of (Fay and McKinley, 2014), in preference to static geographic boundaries or physical definitions based on ocean dynamics (e.g. fronts). This approach combines large-scale physical and biogeochemical characteristics to delineate regions of biogeochemical similarity (biomes). ~~BIOPERIANT12 mean biomes (Fig. 6a) were calculated using the model's climatological~~

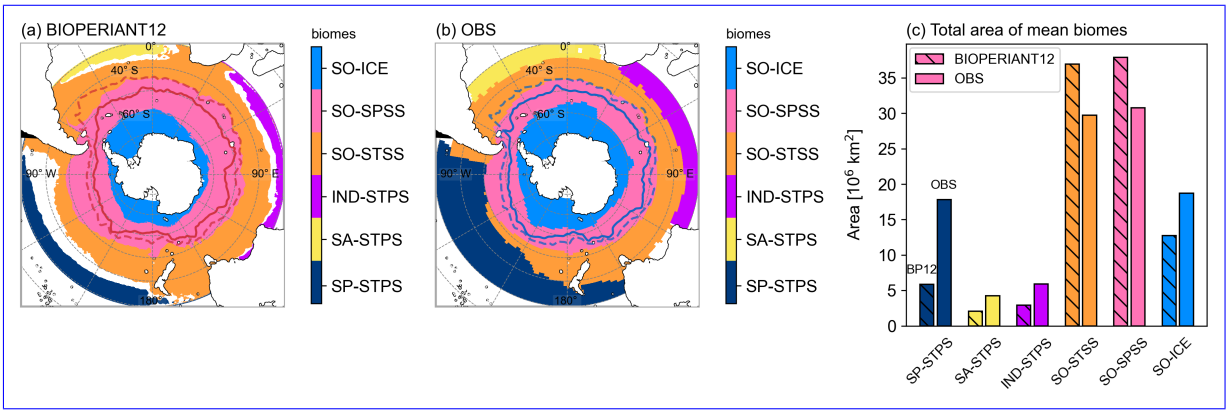

Figure 6. SO mean biome boundaries for **(a)** BIOPERIANT12 using the biome criteria definitions from Fay and McKinley (2014), **(b)** the observation-based mean biome dataset of Fay and McKinley (2014) south of 30° S (see Supplementary), and **(c)** total area per biome for BIOPERIANT12 (hatched bars, titled BP12) and for the dataset (plain bars, titled OBS). In the SO (below 30° S), six biomes are identified: SO-ICE, SO-SPSS, SO-STSS, IND-STPS, SA-STPS and SP-STPS. Annual mean frontal positions of SAF and PF are overlaid.

Biomes are derived from climatological fields of sea surface temperature (SST), ~~Chlorophyll-a, MLD~~ sea ice fraction, spring/summer chlorophyll-a, and maximum mixed layer depth (MLD), using criteria defined in Fay and McKinley (2014, Table 1). SST and sea ice fraction ~~fields. The Fay and McKinley (2014) biome product based on 1998–2010 climatology (Fig. 6b)will be used to aggregate observational data. We thus compare similar, biophysically consistent SO regions between the simulated variables and the observations for the following biomes :~~ criteria are used to distinguish between ice-covered, subpolar, and subtropical zones, while chlorophyll-a and MLD criteria reflect environmental controls on biological production, such as vertical mixing, stratification, and seasonality (i.e. permanent vs. seasonal stratification).

Within the BIOPERIANT12 domain, the following biomes are identified (Fig. 6): in the SO, the ice biome (SO-ICE), the subpolar seasonally stratified biome (SO-SPSS), and the subtropical seasonally stratified biome (SO-STSS)~~. Other southern hemisphere biomes were not considered, ~~; further north, the subtropical permanently stratified biomes of the South Pacific (SP-STPS), South Atlantic (SA-STPS), and Indian Ocean (IND-STPS). A comparison between the BIOPERIANT12 ~~does not fully capture the subtropical mean state~~ biome distribution (Fig. 6a) and the observational product from Fay and McKinley (2014, Fig. 6b) shows that the model underrepresents the subtropical permanently stratified biomes (SP-STPS, SA-STPS~~and ~~, IND-STPS)~~which results in about ~~, resulting in approximately 60 % less area coverage than ~~the corresponding observedbiomes and slightly overestimates ~~observed. Conversely, the SO-STSS ~~, and SO-SPSS biomes are slightly overestimated (Fig. 6c). ~~Thus, the biome criteria ~~As a result, only the SO biomes are used for subsequent aggregation and analysis. The observed differences may suggest some ~~of the ~~model–observation gaps (Fig. S9, S10) as well as ~~address the effect of mesoscale features that are resolved in the higher resolution model compared to the gridded data used in the Fay and McKinley (2014) biome productand is ~~the influence of mesoscale variability resolved by the model but absent from the coarser gridded datasets used to derive the observational biome product. This is further discussed in the Supplementary.

3.2.2 Biome characteristics

To characterise the seasonal cycle ~~of~~ in the model, we present Fig. 7 the surface mean seasonal cycle of selected variables for each SO biome~~(Fig. 7) and biome-mean metrics in Table 3 (Table S1 for 200 m). To~~ . To further contextualise the upper water column~~of the biome, particularly the influence on surface pin highly seasonally stratified areas, ,~~ vertical profiles per biome are ~~provided~~ shown in Fig. S11. In Table 3, ~~the biome-mean seasonal cycle for model and observations (as shown in Fig. 7) are given by~~ we summarise the seasonal cycle at the surface using the mean and amplitude (difference between ~~the~~ minimum and maximum~~values). To compare the model's seasonal cycle and that of the observational data, we used~~), along with statistical metrics used to evaluate model–data agreement: the correlation coefficient ~~between model and data~~ (R), the ratio of standard ~~deviation~~ deviations (RSD), ~~model Reliability Index~~ the model reliability index (RI), and ~~Seasonal Cycle Reproducibility~~ the seasonal cycle reproducibility (SCR). The ~~RSD shows how the model variability~~ same metrics are provided for 200 m depth in Table S1.

The correlation coefficient quantifies how well the timing and shape of the model seasonal cycle matches the observations. The RSD indicates how well the magnitude of seasonal variability in the model compares to that ~~expected by the observed dataset,~~ of the observations, with a value of ~~one suggests they compare well. We highlight certain regions in the model which are inconsistent with data by regions where the model variability exceeded that of observations by 50 % and where model variability was less than 50 % of the expected variability. The model RIor geometric root-mean~~ 1.00 representing comparable variability between the two. The RI, or geometric root mean square error (Leggett and Williams, 1981; Doney et al., 2009), ~~gives the~~ measures the normalised model–data bias ~~that is normalised to the data and used for data that are~~ for log-normal distributed ~~,~~ variables, with a value of ~~one indicates perfect agreement , while two indicates that the error is of similar~~ 1.00 indicating perfect agreement and 2.00 implying model error is comparable in magnitude to the data. ~~The metric SCRis defined in Thomalla et al. (2011)~~SCR, defined by Thomalla et al. (2011), measures how well the climatological seasonal cycle captures the year-to-year evolution of a variable. It is calculated as the correlation ~~coefficient of the interannual varying time series at its full temporal resolution against its~~ between the full-resolution time series and its climatological seasonal cycle (see Fig. S12 for further explanation)~~, i.e. how well the mean climatological seasonal cycle represents the evolution of a property over each year. SCR higher than~~ . SCR values above 0.85 ~~defines a region of high SCR (e.g. high seasonality),~~ indicate high seasonality, between 0.65~~to 0.85 medium SCR~~ –0.85 medium seasonality, and below 0.65 ~~, low SCR (e.g. low seasonality). The SCR for observational products were only calculated if they had an~~ low seasonality. SCR was only calculated for observational datasets with adequate temporal resolution (i.e. higher than monthly).

~~SO mean biome boundaries for **(a)** BIOPERIANT12 using the biome criteria definitions from Fay and McKinley (2014), **(b)** the observation-based mean biome dataset of Fay and McKinley (2014) south of 30S (see Supplementary). **(c)** Total area per biome for BIOPERIANT12 (hatched bars, titled BP12) and for the dataset (plain bars, titled OBS). In the SO (below 30S), six biomes are identified: the ice biome (SO-ICE), the subpolar seasonally stratified biome (SO-SPSS), the subtropical seasonally stratified biome (SO-STSS) and the Indian, South Atlantic, and South Pacific subtropical permanently stratified biome (IND-STPS, SA-STPS and SP-STPS respectively).~~

~~High resolution observations show that the seasonal response of BGC to physical forcing in the SO are regionally dependent.~~ Model–data ~~agreement results~~ differences can result from a combination of factors~~: the available/applied observational dataset~~ ~~(listed in~~ , including the characteristics and limitations of the observational datasets (Table 1)~~; which carries uncertainty due to poor sampling/spatiotemporal resolutionand are oftentimes interpolated into gridded products and only available as climatologies; the application of biome definitions over~~ , which often suffer from sparse sampling, low temporal and spatial resolution, and interpolation. Additional differences may arise from applying biome definitions to regions of high variability~~(EKE) which is not used for biome definition but is shown to improve~~ /EKE. Although EKE is not explicitly included in the biome classification, it has been shown to reduce partial pressure of carbon dioxide (pCO_2~~bias~~) biases and root mean square ~~error (Gregor et al., 2019); and the effect of~~ errors (Gregor et al., 2019). Further uncertainty is introduced through area-weighted ~~, domain averaging over large regions/~~domain averaging across large biomes. In contrast to regions dominated by intraseasonal variability, where observations are more difficult to constrain (Monteiro et al., 2015), the seasonal cycle metrics are expected to ~~agree with the data in regions where the response of the model is also seasonally driven with high SCR~~show stronger model data agreement in regions with seasonally driven dynamics (high SCR).

In general, the metrics (Table 3, Fig. 7) show the model's seasonal cycle agrees ~~with that of the~~ well with that the observed data, for example, the temperature seasonal cycle per biome is well represented~~, however, a reasonable comparison with the data is expected since~~ . However, given that temperature is a criterion used in the biome definition~~. We, therefore,~~ , a reasonable agreement is expected. Therefore, we focus on the ~~model-observation disagreements~~ model–observation discrepancies, which highlight regions of interest. For the dynamics, there is a poor correlation of salinity in the SO-STSS region (R = 0.62), ~~this~~ which could be associated with the high mesoscale spatial and temporal variability in the model (low seasonality ~~of~~ SCR = 0.12)~~in the model compared with data. While in~~ . In the SO-ICE biome, high variability in salinity (RSD = 1.55), MLD (RSD = 1.56) as well as dissolved O_2 (RSD = 1.66) ~~, point at the influential role~~ to the significant influence of sea ice and freshwater dynamics in the model~~region and suggest improvement~~ . This suggests that improvements or further investigation may be needed. For the BGC, poor model reliability for carbon, silicate, and chlorophyll~~as well as deviations in nutrients~~ , along with deviations in nutrient concentration, will be addressed in the proceeding sections.

Table 3. Seasonal cycle surface climatology per biome: BIOPERIANT12 (BP12) vs. observations (OBS)~~: area-weighted~~ . Area-weighted Mean and Amplitude (difference between maximum and minimum) are shown for ~~the respective~~ each data ~~sources~~source; SCR is the seasonal cycle reproducibility (~~the~~ correlation of the interannual varying ~~timeseries against~~ time series with its climatological seasonal cycle) where temporal resolution allows; and for comparison Correlation (correlation coefficient), RSD (ratio of BP12:OBS standard deviation), and Model Reliability Index (log-transform error) ~~.~~are included

Variable								Variable							
	Biome	SO-ICE		SO-SPSS		SO-STSS			Biome	SO-ICE		SO-SPSS		SO-STSS	
		BP12	OBS	BP12	OBS	BP12	OBS			BP12	OBS	BP12	OBS	BP12	OBS
Temperature	Mean	-1.49	-1.00	3.03	3.76	13.45	12.75	Salinity	Mean	34.03	33.96	34.01	33.93	34.83	34.71
$[°C]$	Amplitude	1.16	1.82	2.36	2.74	3.90	4.25		Amplitude	0.70	0.43	0.08	0.08	0.01	0.06
	SCR	0.63		**0.71**		0.54			SCR	0.35		0.20		0.12	
	Correlation		0.94		0.98		0.99		Correlation		0.99		0.84		0.62
	RSD	0.66		0.90		0.93			RSD	**1.55**		1.07		**0.14**	
	Model RI	**2.32**		1.26		1.06			Model RI	1.00		1.00		1.00	
MLD	Mean	66.72	57.02	109.79	109.08	86.20	100.53	Tot. chl-a	Mean	0.58	0.28	0.51	0.24	0.61	0.35
[m]	Amplitude	86.87	54.57	143.26	118.04	153.40	158.03	$[mgm^{-3}]$	Amplitude	1.69	0.70	0.88	0.23	0.75	0.21
	SCR	**0.76**		**0.74**		**0.75**			SCR	**0.88**	0.36	**0.85**	0.36	**0.68**	0.21
	Correlation		0.86		1.00		1.00		Correlation		0.93		0.86		0.91
	RSD	**1.56**		1.19		0.95			RSD	**2.37**		**4.22**		**3.64**	
	Model RI	1.41		1.11		1.31			Model RI	**1.86**		**2.10**		**1.69**	
pCO_2	Mean	345.25	367.37	363.98	365.15	362.96	345.27	FCO_2	Mean	-0.82	0.15	-1.12	-0.07	-0.77	-1.81
$[\mu atm]$	Amplitude	49.30	47.90	10.22	17.10	13.08	11.85	$[molm^{-2}yr^{-1}]$	Amplitude	2.17	1.80	1.17	1.48	1.54	0.45
	SCR	**0.79**	**0.79**	0.59	**0.80**	0.51	**0.83**		SCR	0.39	**0.77**	0.31	**0.80**	0.28	**0.76**
	Correlation		0.89		**-0.45**		**-0.59**		Correlation		0.89		**-0.78**		**-0.23**
	RSD	0.91		0.65		1.06			RSD	1.30		0.80		**3.53**	
	Model RI	1.07		1.02		1.06			Model RI	**3.87**		**2.59**		**6.37**	
DIC	Mean	2181.93	2148.95	2151.61	2123.52	2087.99	2056.03	Tot. Alkalinity	Mean	2303.80	2295.51	2295.77	2281.70	2317.60	2300.31
$[\mu molkg^{-1}]$	Amplitude	62.96	0.00	15.50	0.00	23.00	0.00	$[\mu molkg^{-1}]$	Amplitude	43.62	0.00	3.67	0.00	4.02	0.00
	SCR	0.53		0.44		0.47			SCR	0.50		0.29		0.21	
	Correlation				**0.00**		**0.00**		Correlation		**-0.00**				
	RSD								RSD						
	Model RI	1.02		1.01		1.02			Model RI	1.01		1.01		1.01	
Nitrate	Mean	26.02	25.73	23.04	21.75	10.52	6.83	Phosphate	Mean	1.85	1.81	1.63	1.56	0.80	0.68
$[mmoll^{-1}]$	Amplitude	3.92	3.69	1.91	2.73	3.77	3.52	$[mmoll^{-1}]$	Amplitude	0.22	0.26	0.10	0.32	0.21	0.33
	SCR	0.58		0.46		0.61			SCR	0.56		0.42		0.55	
	Correlation		0.95		0.95		0.97		Correlation		0.99		0.90		0.92
	RSD	1.28		0.73		1.24			RSD	0.86		**0.36**		0.67	
	Model RI	1.02		1.06		**1.55**			Model RI	1.03		1.07		1.22	
Silicate	Mean	48.47	53.42	26.46	15.85	5.81	3.37	Diss. O_2	Mean	357.13	347.78	332.14	326.98	264.86	274.04
$[mmoll^{-1}]$	Amplitude	13.96	12.44	5.47	11.30	2.70	2.70	$[\mu moll^{-1}]$	Amplitude	29.65	21.34	13.77	14.52	17.08	16.90
	SCR	0.64		0.49		0.62			SCR	0.53		0.45		0.47	
	Correlation		0.85		0.96		0.95		Correlation		0.86		0.94		0.99
	RSD	1.18		**0.49**		1.05			RSD	**1.66**		0.91		0.95	
	Model RI	1.12		**1.79**		**1.79**			Model RI	1.03		1.02		1.03	

[a] GLODAPv2 observations are an annual mean product.

RSD:SD of BP12 greater (less) than that of OBS by factor 1.5 (0.5). **Correlation**: BP12-OBS correlation coefficient less than 0.5.

SCR: BP12 greater than 0.65 (medium to high). **Model RI**: greater 1.5 (medium to high).

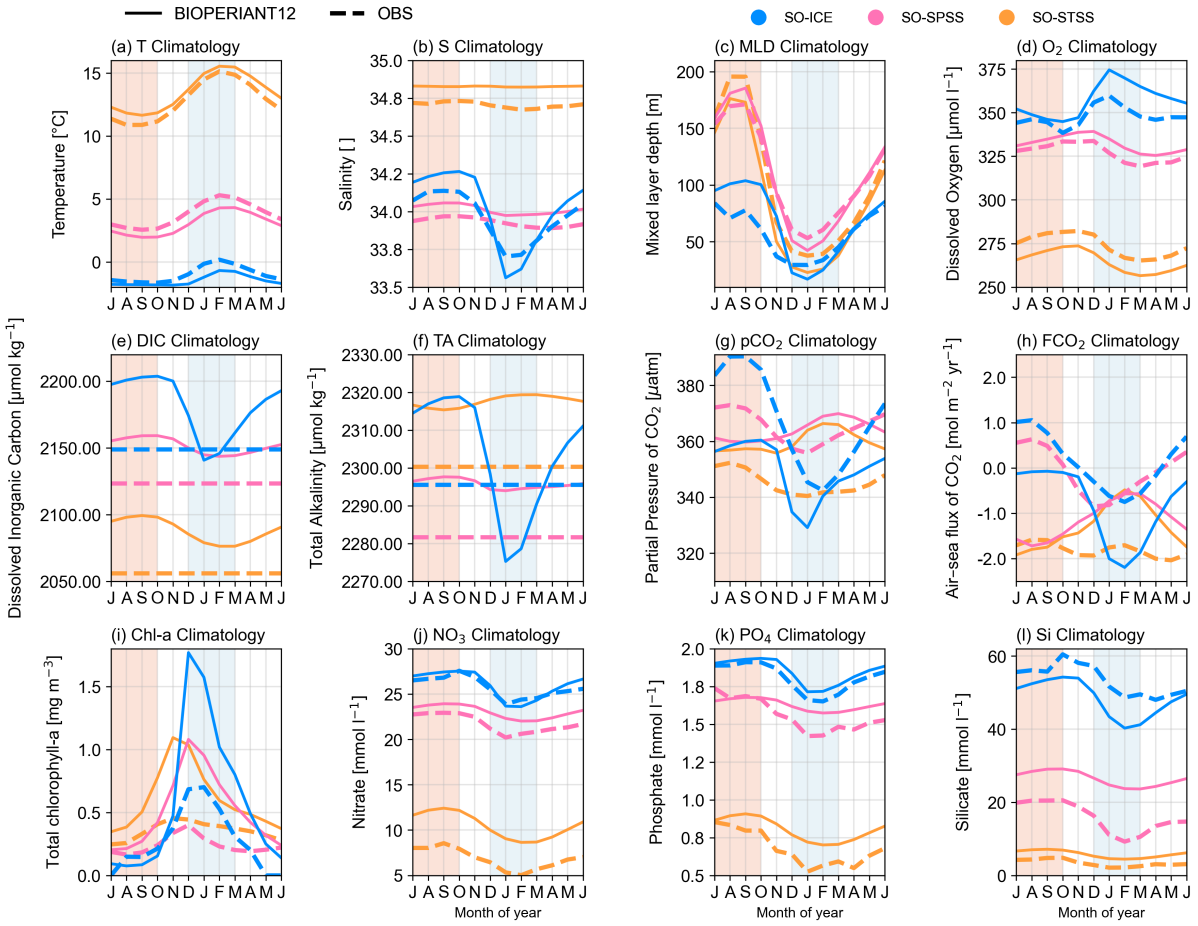

Figure 7. BIOPERIANT12 model (solid line) ~~versus Observations~~ vs. observations (dashed line) surface seasonal cycle (2000–2009 climatology) spatially averaged per biome for selected variables. Biomes include SO-ICE (blue), SO-SPSS (pink) and SO-STSS (orange), corresponding to the map in Fig. 6.

3.3 Carbon

Recent studies have highlighted the importance of resolving intra-seasonal to seasonal ~~modes of~~ variability for both anthropogenic and natural carbon fluxes in order to reduce ~~the uncertainties of the~~ uncertainties in mean annual fluxes and ~~strengthen~~ improve model projections (DeVries et al., 2023; Rustogi et al., 2023). We compare BIOPERIANT12 pCO_2 to the monthly observation-based product CSIR-ML6 (Table 1). CSIR-ML6 is a gridded 1° x 1° machine learning-based reconstruction of surface ocean pCO_2, derived from Surface Ocean CO_2 Atlas (SOCAT, Bakker et al., 2016) observations and satellite-based environmental predictors (Gregor et al., 2019).

Using SCR, as a metric of variability, a comparison ~~of the SCR of pCO2 in~~ between BIOPERIANT12 ~~against the monthly, data product~~ and CSIR-ML6 (Fig. 8) shows that model pCO_2 for the SO-STSS and SO-SPSS biomes ~~are~~ is dominated by large regions of interannual variability (SCR = 0.59, 0.51, respectively), aligned with regions of high EKE (Fig. 2) which are not captured by the monthly CSIR-ML6 product (Fig. 8c). CSIR-ML6, instead, displays high seasonality in all three SO biomes with SCR values of 0.80, 0.80, 0.79 in the SO-STSS, SO-SPSS, SO-ICE biomes, respectively (Table 3)~~, i.e.~~. These patterns are largely driven by seasonal surface fluxes and ~~ice (~~sea ice, although the monthly ~~temporal resolution may contribute to this)~~resolution of CSIR-ML6 may also contribute to the stronger seasonality.

This results in dissimilar pCO_2 seasonal cycles (Fig. ~~g)highlighted~~ 7g), as shown by weak correlations in the SO-STSS and SO-SPSS biomes (R = ~~-0.59, -0.45, respectively)whilst showing~~ –0.59 and –0.45, respectively), in contrast to good model–data agreement in the SO-ICE biome~~; a region that~~. The SO-ICE biome is also strongly seasonally driven in the model (SCR = 0.79 ~~,~~ for both model and data) and ~~with~~ shows coherent model–data phasing (R = 0.89), although ~~minima are one month out of phase. Despite biome mean differencesin the model climatology, we calculate a~~ the seasonal minima are offset by one month. Despite these differences, the small model–data bias ~~of~~ in pCO_2 ~~for all 3 biomes indicated by model~~ across all three biomes (RI between 1.02 ~~to~~ and 1.07~~, which suggests that BIOPERIANT12 is in agreement with the data product CSIR-ML6; also shown in the~~) and the broadly overlapping Probability Density Functions (PDFs) for ~~pfor~~ the SO domain mean pCO_2 (Fig. S13a) ~~. This emphasises~~ indicate some level of agreement in the mean state. These findings underscore the importance of mesoscale-resolving model resolution in the SO ~~, in~~ for capturing the variability of CO_2.

The spatial distribution of pCO_2 shown in Fig. 9 (a–f) ~~reflects the seasonality differences between~~ illustrates the seasonal differences between the model and observations, with the model ~~and data, showing the overestimation of model versus data~~ tending to overestimate pCO_2 in the SO-STSS and ~~underestimation~~ underestimate it in the SO-ICE biomes. ~~Differences in seasonal cycle phasing~~ Seasonal cycle phasing differences in the SO-SPSS and SO-STSS biomes are ~~clearly seen~~ apparent in the interannual time series (Fig. 9i, k)~~with~~ , where the model peaks in summer~~compared~~ , in contrast to winter peaks in the data. The PDFs for pCO_2 (Fig. 9h, j, l) show ~~a general wider distribution (~~generally broader distributions (i.e. higher standard deviation) in the model ~~biomes and not the distinct~~ across all biomes , whereas the data exhibit clearer inter-biome ~~differences shown in the data~~ distinctions, such as the ~~narrow~~ narrower pCO_2 distribution in the SO-SPSS (Fig. 9j).

The seasonal cycle differences of pCO_2 (and FCO_2) in the model SO-SPSS and SO-STSS biomes~~relative to these observationsmay be representative of different mechanisms. The~~ , relative to observations, may reflect the influence of different controlling

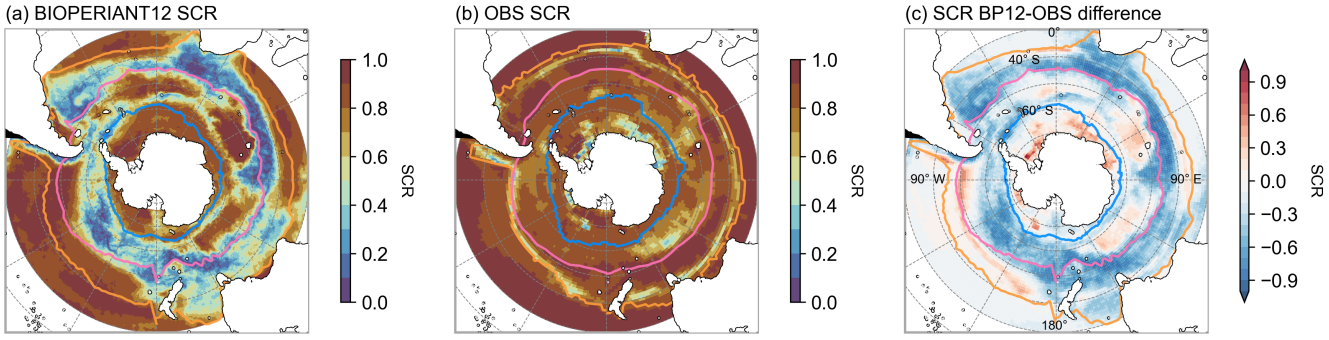

Figure 8. Seasonal cycle reproducibility of pCO_2 for **(a)** BIOPERIANT12 , **(b)** CSIR-ML6 ~~observation based~~ observation-based reconstruction, and **(c)** model–data difference. Maps are overlaid with the northern ~~climatological~~ mean biome borders corresponding to model/data SO biomes.

mechanisms. In these biomes, the modelled pCO_2 seasonal maximum occurs in summer (JFM)~~is~~ , in phase with the temperature maximum (Fig.7a), but out of phase with the chlorophyll peak~~2~~ , which occurs about two months earlier (OND) (Fig.7i, 13)~~and associated nutrient decrease~~ , and with the associated nutrient drawdown (NO_3 and Si~~,~~ ; Fig.7j, l). This ~~is consistent with the model's pseasonal cycle~~ suggests that in the SO-SPSS and SO-STSS biomes~~being primarily regulated by the thermal component~~ , the seasonal cycle of pCO_2 ~~(Mongwe et al., 2016). On the other hand, there is better model–data phasing of~~ in the model is primarily driven by the thermal component (Mongwe et al., 2016). By contrast, the seasonal cycles of pCO_2 and FCO_2 in the SO-ICE biome show better phasing between model and data (Fig.7g, h)~~. Additionally,~~ , and the seasonal cycles of temperature, chlorophyll, and ~~nutrient model-data seasonal cycles are comparable in phase~~ nutrients are also more closely aligned (Fig.7i–l). However, the amplitude of the ~~BIOPERIANT12~~ seasonal chlorophyll maximum ~~is~~ in the model is approximately double that of the observed estimate ~~(due to~~ across all biomes. The climatology maps (Fig. 11) show that the model's overestimation aligns with regions of high chlorophyll ~~, Fig. 11) which may result in~~ in the data, which may lead to a larger contribution of ~~the~~ biological components driving pCO_2~~as compared to the thermally driven ice free regions~~, particularly in the SO-ICE biome.

It is ~~noted~~ important to note that observational products, particularly those based on underway pCO_2 observations used in reconstructions, ~~have~~ carry significant seasonal biases ~~themselves, as they are based on limited observations during winter . Thus, the~~ due to sparse coverage during winter months. Consequently, the true magnitude and direction of the observed seasonal cycle of pCO_2 and FCO_2 in the SO ~~is still under investigation (Gray et al., 2018; Landschützer et al., 2018; Gregor et al., 2019; Gruber et al., 201~~ ~~. The seasonal biases in these products may also manifest as artificial variability on longer time scales~~ remain uncertain (Gray et al., 2018; Landschützer et al., 2018; Gregor et al., 2019; Gruber et al., 2019; Bushinsky et al., 2019; Mackay and Watson, 2021) . These seasonal sampling biases may also propagate into longer-term variability artefacts in the reconstructions (Hauck et al., 2023). The ~~poor representation of biological processes of the~~ discrepancies between BIOPERIANT12 and the observational products, particularly in the SO-SPSS and SO-STSS ~~in the modelcontributing to differences in the p(and F) seasonal cycles~~

is biomes, may also reflect the model's limited representation of key biological processes (discussed in the Supplementary). We propose that a weaker seasonal vertical flux in DIC as shown by the smooth upper ocean of DIC in the model, shown by a smoother upper-ocean DIC gradient compared to the dataset (Fig. S11)leads to a weaker DIC entertainment potential during the seasons , reduces the potential for DIC entrainment during periods of enhanced vertical mixing, and hence a diminished seasonal DIC variability thereby dampening the seasonal variability of DIC (Mongwe et al., 2016).

3.4 Biogeochemistry

3.4.1 Dissolved Iron

Dissolved iron (dFe) limits phytoplankton growth across the surface of the SO, impacting the functioning of marine ecosystems andthus , consequently, the carbon cycle. It is thus therefore imperative that models adequately accurately represent the spatial and seasonal distribution of dFe. In the SO, dFe is notoriously undersampled, it occurs at small low (nanomolar, n M) concentrationsnM) concentrations, and its complex chemistry makes it difficult to observe. Here, we compare BIOPERIANT12 with a compilation of dFe observations collated by Tagliabue et al. (2012) over 2000–2009 (Fig. 10). BIOPERIANT12 simulates captures the observed spatial distribution of upper ocean dFe concentrations, with higher concentrations elevated levels (> 0.4 n Mclose to) near coastal boundaries, downstream and around subAntarctic sub-Antarctic islands (particularly evident for around Kerguelen), and in the vicinity of the Agulhas Retroflection (Fig. 10a, c). Far from the influence of In regions distant from land masses, the simulated dFe concentrations are lower (< 0.3 n M, as similarly), seen in the observations (Fig. 10b). In generalOverall, the simulated range of upper dFe is open ocean surface dFe range lies on the lower end of the range of the observations; it has been noted observed spectrum; this is consistent with previous findings that PISCES tends to exaggerate the low dFe concentrations in the open ocean of the SO (Aumont et al., 2015)underestimate open ocean dFe in the SO. This is suggested to arise from the simplification of the biological processes in the model that affects iron cycling and supply (Aumont et al., 2015; Tagliabue et al., 2016; Nicholson et al., 2019).

The shape of the vertical profile of dFe dFe profile is important as it plays a fundamental role in how much dFe is available to determines the amount of dFE that can be supplied to the surface i.e. via ocean through processes such as deep winter convective mixing and by mesoscale eddies mesoscale eddy activity (Tagliabue et al., 2014; Nicholson et al., 2019). BIOPERIANT12 is able to simulate the mean observed characteristics of a general reproduces the general features of the observed dFe profile (Fig. 10e), with low concentrations between 0-100 m due to biological consumptionand increasing DFe in the upper 0–100 m from biological consumption, and increasing concentrations with depth due to remineralization remineralisation of sinking organic material. The simulated mean range dFe compares relatively well with mean observations over Simulated dFe values compare reasonably well with observations in the upper 500 m. Below this, the simulated mean range is lower . The lack , but tend to be lower at greater depths.

The scarcity of measurements during key seasonal transitions, particularly over winter (Fig. 10f)make comparisons , limits robust evaluation of the simulated seasonal distribution of surface dFedifficult. However, during surface dFe. Nevertheless, austral summer (DJF) , dFe is expected to be low exhibit low surface dFe due to biological consumption from spring to

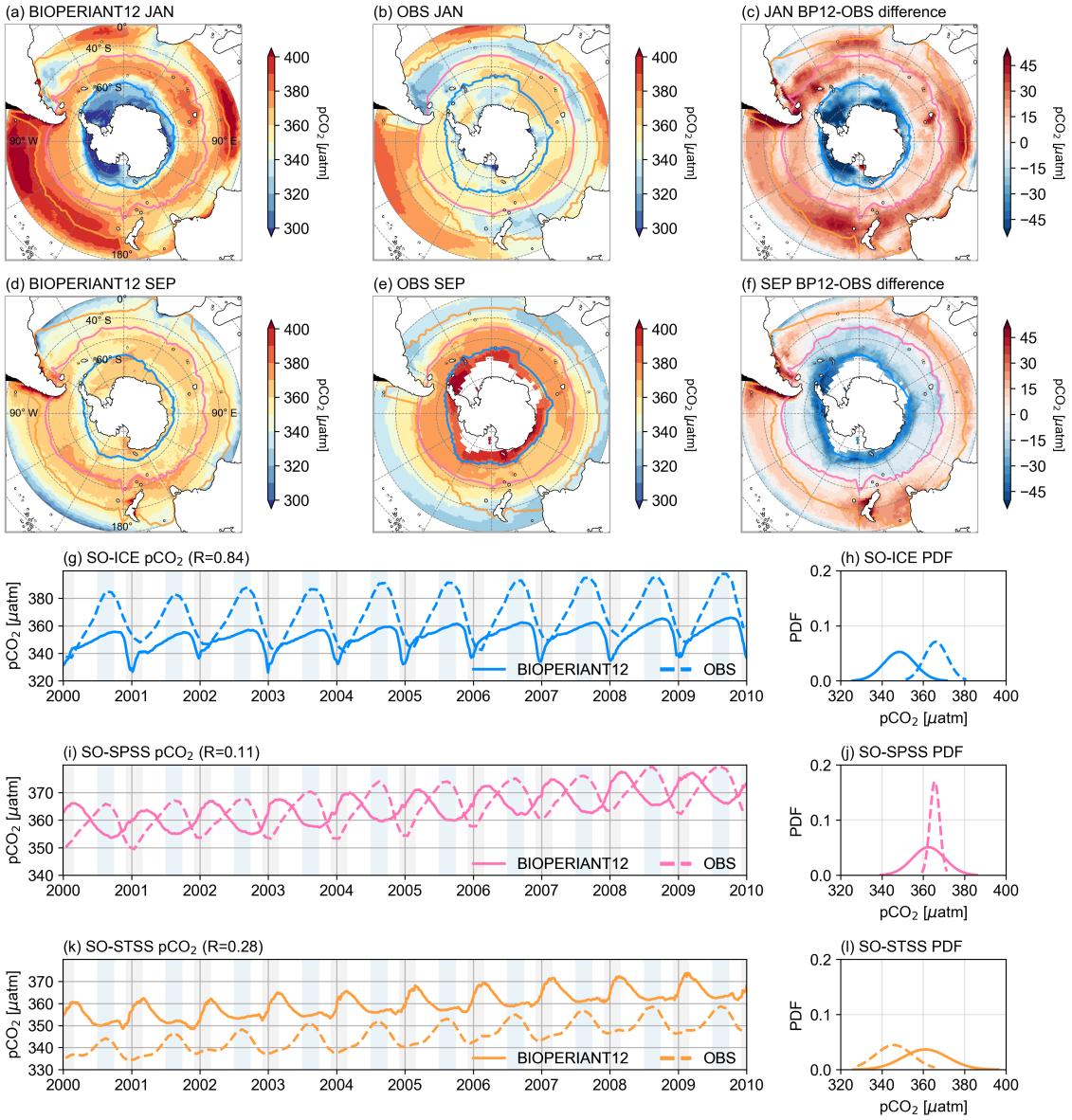

Figure 9. Seasonal comparison (January vs. September climatology) of pCO_2 for **(a, d)** BIOPERIANT12, ~~and~~ **(b, e)** the CSIR-ML6 observation based dataset, and **(c, f)** the model–data difference~~, for January and September monthly climatology, respectively~~. Maps are overlaid with the northern ~~climatological~~ mean biome borders corresponding to model/data SO biomes. Evolution of area-weighted pCO_2 for model ~~versus~~ vs. data and ~~correspnding~~ corresponding PDF for **(g, h)** SO-ICE, **(h, i)** SO-SPSS, and **(k, l)** SO-STSS biomes.

summer~~and during~~ , while winter (JJA) ~~, dFe~~ is expected to ~~be higher due to~~ show higher surface dFe as a result of vertical entrainment of subsurface iron during deep convective mixing ~~entraining subsurface dFe to the surface (Tagliabue et al., 2012)~~

~~These seasonal differences are simulated~~ (Tagliabue et al., 2012). These seasonal variations are captured by BIOPERIANT12 (Fig. 10f)~~and are particularly evidenced by~~ , as also shown in the summer and winter distribution snapshots in Fig. 10c and d, respectively.

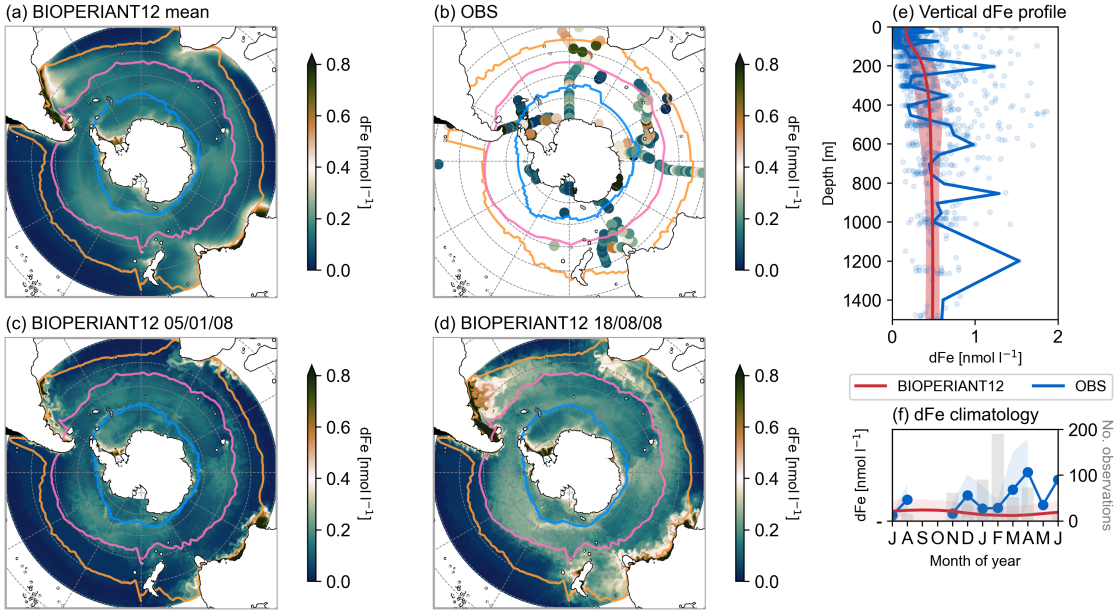

Figure 10. Surface (~~0–50~~ 0–50 m) dissolved iron (dFe) concentration for **(a)** BIOPERIANT12 ~~climatological~~ annual climatological mean **(b)** observations ~~obtained during years 2000–2009~~ from 2000–2009 (Tagliabue et al., 2012). Seasonal snapshots of BIOPERIANT12 dFe for **(c)** summer (5 January 2008) and **(d)** winter (18 August 2008). **(e)** ~~Annual~~ Climatological mean vertical distribution of dFe for BIOPERIANT12 ~~without area-weighting~~ (red line = mean~~,~~ ; red shading = spatial standard deviation) and observations (blue). **(f)** Model ~~versus~~ vs. observation monthly ~~mean~~ climatology (~~line~~lines) and standard deviation (shading)~~. The~~ ; the number of observations ~~in each~~ per month is shown by grey bars.

3.4.2 Nutrients

Model RI values in Table 3 ~~show that the model~~ indicate that BIOPERIANT12 is able to reasonably reproduce the seasonal climatology of NO_3 and PO_4 with relatively comparable seasonal cycles (Fig. 7), particularly ~~for~~ in the more southern biomes (e.g. RI values between 1.02 and 1.07 for both NO_3 and PO_4 in the SO-ICE and SO-SPSS biomes). However, simulated surface ~~silicate~~ Si is less well represented ~~by the model (SO–SPSS and SO–STSS both~~ (RI = 1.79 for both SO-SPSS and SO-STSS): in the ~~SO–SPSS, model silicate means differ compared to data~~ SO-SPSS, the model mean Si concentration (26.46 ~~vs.~~ mmol l^{-1}) is substantially higher than observed (15.85 mmol l^{-1}), ~~considering their amplitudes~~ with a reduced seasonal amplitude (5.47 vs. 11.3 mmol l^{-1}) and ~~variability that is half that of the data~~ only half the variability (model RSD = 0.49). These ~~differences may result from the representation of simulated silicate due to uncertainty in laboratory experiments as noted in~~

Aumont et al. (2015). This mayaffect the concentration of diatoms in the model. PO_4 variability in the model is also low, 0.36 times that expected of data however, with comparable meansdiscrepancies may stem from uncertainties in the silica dissolution process and its formulation in the model Aumont et al. (2015), which may, in turn, affect the simulated diatom distribution.

While model PO_4 exhibits reasonable mean values, its variability is also underestimated, at only 36 % of that observed. It is important to note that much of the observational data is collected during dataset is biased towards the productive season (austral summer) in the SO, and thus surface values observed may be biassed towards lower which may result in lower observed surface nutrient values (Fig. 7, S16). However, deeper in the water column at

At 200 (Table S1, Fig. S17), RIs for the 3 aforementioned nutrients reflect a good agreement between the modeland observations at this level (m depth, however, RI values for all three nutrients indicate good model–data agreement (ranging between 1.00 and 1.30). Model nutrients ; Table S1, Fig. S17). Nutrient concentrations at this depth are stable , in the model, with standard deviations smaller than from the data climatology as in the vertical profiles those from the observational climatology (Fig. S11). Over the evolution of the model model simulation period (Fig. S16 and S17), there is a slight decreasing trend in nutrientsdeclining trend in nutrient concentrations, particularly noticeable in the SO-SPSS both at the surface and at 200 and m, which should be taken into account consideration in process studies.

3.4.3 Surface chlorophyll

To evaluate the model's representation of biological variability, we compare surface chlorophyll concentrations from BIOPERIANT12 represents the main spatial surface patterns of regions of higher and lower surface chlorophyll as compared to OC-CCIv6 with the OC-CCI v6 satellite-derived dataset (Table 1) gridded at a comparable resolution of 9 km and aggregated weekly to match the model output. BIOPERIANT12 broadly captures the spatial patterns of surface chlorophyll concentrations (Fig. 11). For example, it simulates the higher surface chlorophyll close to the model captures enhanced chlorophyll levels near continental margins and in the region of ocean fronts such as in the SAZ (frontal regions such as the Subantarctic Zone (SAZ; not shown), while low chlorophyll is lower chlorophyll concentrations are simulated in more oligotrophic regions such as the SO Pacific like the South Pacific sector of the SO. However, the there are notable differences in the summer pattern (Fig. 11a–c), such as the overestimation of the spatial extent of enhanced chlorophyll regions elevated chlorophyll concentrations associated with shallow topographyare larger in the model. The incorporation of these regions within the biome definitions contribute to the magnitude of the surface chlorophyll which is overestimated in BIOPERIANT12, with variability over double that of the observations in all biomes (RSD greater than 2 in Table. While the overestimation of chlorophyll occurs regardless of spatial aggregation, the inclusion of these elevated regions within biome definitions contributes to the overestimation of biome-mean values and results in variability more than twice that observed (RSD > 2.00 in Table 3).

Climatological mean total chlorophyll concentrations for **(a, b)** BIOPERIANT12 vs **(d, e)** OC-CCI observation-based product for January and September. SCR of surface chlorophyll for **(c)**BIOPERIANT12 and **(f)** observations. Model versus observation seasonal cycle of surface chlorophyll for **(g)** SO-ICE, **(h)** SO-SPSS, and **(i)** SO-STSS biomes.

SCR (Fig. 12) suggests that the drivers of the differences are from dynamics as model chlorophyll is seasonally driven while the data product suggests that drivers are on the intraseasonal time-scale. Despite this, the seasonal cycle for the SO biomes

correlates well with data. A comparison of the simulated biome-mean seasonal cycle against observations of the overestimation of model chlorophyll arises from the temporal variability : the response of model chlorophyll is strongly seasonal, whereas satellite indicates strong intra-seasonal variability. Nevertheless, BIOPERIANT12 shows good agreement with OC-CCIv6 chlorophyll for each biome in terms of the climatological seasonal cycle (Fig. 13a–c, S18)shows good agreement of 7i), with correlations greater than 0.86 in all SO biomes, and the timing of the bloom maximum peak chlorophyll with bloom maxima generally occurring in December (date difference Fig. 13 with timing differences within 14 days). However, the general characteristics, such as . A biome-mean comparison (Fig. 13, S18) further shows that bloom initiation and terminationdate , defined using the biomass threshold method of 5 % (Ryan-Keogh et al., 2023)only compare well for , are reproduced with varying degrees of success. In the SO-STSS region, both initiating biome, both the model and observations show bloom onset in August and terminating decline in May. For the SO-SPSS biome, both the model and observation blooms start in September and while OC-CCIv6 blooms terminate in Marchdatasets agree on a September onset, the model sustains the bloom a further approximately 93 days into June. In contrast, longer than observed, extending into June (vs. March in data). In the SO-ICE biomebloom for both sources terminate , while model–data agree on termination in May, while the simulated bloom starts the model bloom initiates 3 months after observations (October vs. August).

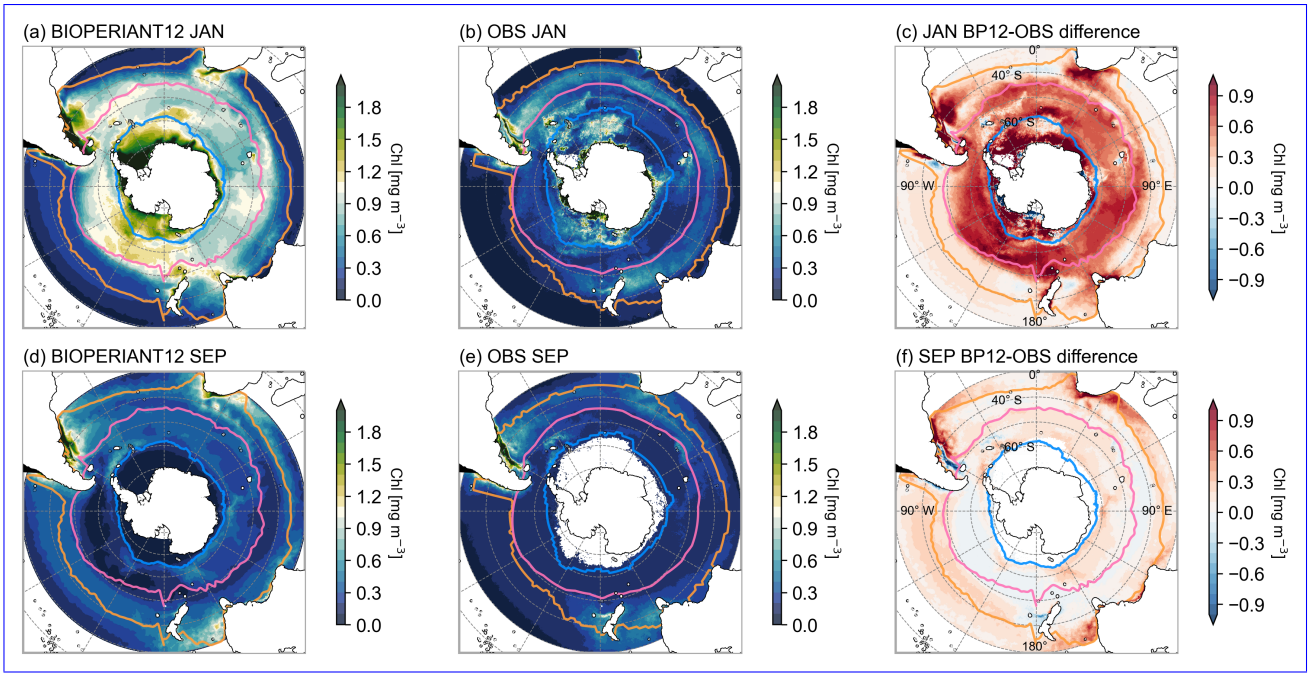

Figure 11. Climatological total chlorophyll concentrations for January and September for **(a, b)** BIOPERIANT12 and **(d, e)** the OC-CCI observation-based product. SCR of surface chlorophyll for **(c)**BIOPERIANT12 and **(f)** observations. Model vs. observation seasonal cycle of surface chlorophyll for **(g)** SO-ICE, **(h)** SO-SPSS, and **(i)** SO-STSS biomes.

These results demonstrate that while BIOPERIANT12 captures key spatial and seasonal features of chlorophyll in the SO, it likely underrepresents the higher-frequency biological variability evident in observations; even at mesoscale-resolving resolution. Underlying ocean dynamics that could be further improved in BIOPERIANT12 include the representation of shelf-slope dynamics and mixing processes. For instance, enhanced vertical mixing may prolong bloom duration, as seen in the SO-SPSS biome, where the modelled bloom persists nearly three months beyond satellite-based estimates. Additionally, the biogeochemical processes that drive productivity and blooms in the SO such as nutrient limitation (especially iron), fixed phytoplankton stoichiometry, and prescribed chlorophyll-to-carbon ratios, also require further refinement. The overestimation of chlorophyll magnitude and mismatches in bloom timing suggest that processes governing phytoplankton bloom dynamics, particularly those modulated by mesoscale physical variability, warrant further investigation.

However, chlorophyll model vs. satellite data comparisons are inherently challenging, with both sources subject to internal biases and uncertainties. Limitations in satellite observations arise from the satellite itself, such as solar zenith angle, cloud cover, and sea ice contamination, particularly at high latitudes; as well as from environmental complexities of the SO like the presence of subsurface chlorophyll maxima and algorithms not well suited to these conditions (Clow et al., 2024; Aumont et al., 2015).

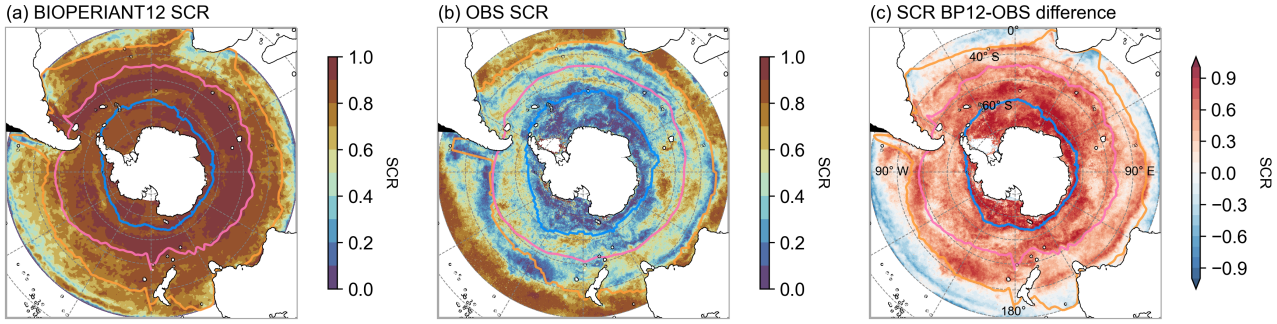

Figure 12. Seasonal cycle reproducibility (SCR) of surface chlorophyll concentration for ~~(a)~~ **(a)** BIOPERIANT12, ~~(b)~~ **(b)** the OC-CCIv6 observation-based product, and ~~(c) model-observation~~ **(c)** model–observation SCR bias.

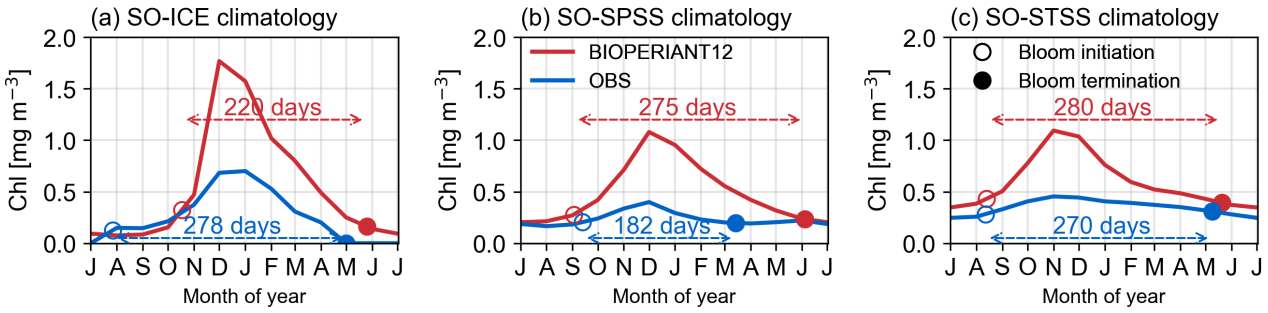

Figure 13. ~~BIOPERIANT12 model versus OC-CCI observation climatological~~ Climatological bloom characteristics from BIOPERIANT12 and the OC-CCI observation-based product overlaid on the seasonal cycle of surface chlorophyll for ~~(a)~~ **(a)** SO-ICE, ~~(b)~~ **(b)** SO-SPSS, and ~~(c)~~ **(c)** SO-STSS biomes.

4 Conclusions

The complex dynamics of the SO ~~has been scrutinised in many papers, particularly with its~~ have been the focus of extensive research, particularly due to their role in the climate system and ~~influence on carbon projections by ESMs. While inter-model comparisons may show the weaknesses and strengths , the models themselves are also complex~~ carbon cycle. While model intercomparisons help expose the strengths and weaknesses of ESMs, individual models remain intricate systems defined by ~~multiple interacting parts defined by many~~ numerous interacting assumptions, making ~~isolating~~ the isolation of specific biases challenging. In contrast, BIOPERIANT12 ~~, on the other hand, while composed of the major components of ocean , ice and biogeochemistry, provides a simpler, stable reference model with a reasonable mean state with which we can address process questions, diagnose model biases, and build future model experiments. Despite the eddying resolution, the simulated SOseasonal cycle still needs improvement. Model-observation differences, not addressed in this evaluation paper, can lead to further paths of enquiry.~~

~~The~~ offers a relatively simpler, high-resolution coupled ocean–ice–biogeochemistry configuration with a stable and realistic mean state as shown by the evaluation of the physical ocean metrics. Thus, providing a useful reference framework for process studies, bias diagnostics, and future model experimentation.

Despite its mesoscale-resolving resolution, BIOPERIANT12 still shows notable limitations in simulating key biogeochemical processes in the SO. In particular, the model overestimates chlorophyll concentrations and exhibits variability more than twice that of satellite-based observations across all SO biomes. The timing and duration of phytoplankton blooms also differ from observations, with blooms sometimes initiating too late or persisting beyond observed termination, as in the SO-SPSS biome. These discrepancies highlight the importance of ~~the mesoscale on biology in the SO requires particular attention with the local environment of the phytoplankton modified through both biological and physical mechanisms, for example by altering gradients and adjusting access to light and nutrients which affect growth and hence the biological carbon pump. Large biomass anomalies in both spatial and seasonally variability are reported in Rohr et al. (2020). In~~ mesoscale processes and their interactions with BGC, such as shelf-slope dynamics, vertical mixing, and nutrient limitation, especially of iron. While some regional biases remain, there are systematic biases attributable to the model formulation and not the configuration design, such as the commonly used fixed chlorophyll-to-carbon ratios and phytoplankton stoichiometry which may limit the model to fully capture the dynamical nature of SO productivity. These issues are common to many biogeochemical models and point to structural limitations beyond just this configuration.

While this model description paper focuses on introducing the BIOPERIANT12 platform and evaluating its large-scale physical and biogeochemical patterns, the use of low-resolution gridded observational datasets inherently limits the depth to which model–data mismatches can be interpreted. In high-resolution configurations such as BIOPERIANT12, ~~chlorophyll variability from two phytoplankton classes (nanophytoplankton and diatoms), averaged over biomes, exceeded observational values by more than double~~discrepancies with observations often reveal limitations, not only in the model formulation but also in the observing systems themselves. BIOPERIANT12 offers an opportunity to diagnose and potentially reduce structural biases; however, doing so requires an equally robust understanding of observational uncertainty.

For physical processes, this has been discussed in the context of the development and constraining of ocean circulation models by Fox-Kemper et al. (2019). In the ~~SO, where biological processes play an important role in carbon exchange, the simulated processes which give rise to these high values need to be explored. Despite the magnitude differences, the temporal variability should also be addressed , the SCR shows that the simulated chlorophyll response is driven by strong seasonal factors, when a higher-temporal response is expected as displayed by the OC-CCIv6 data~~context of BGC, particularly for surface carbon fluxes, understanding the drivers of primary production and bloom dynamics is critical (Thomalla et al., 2023) . Although satellite products have the necessary spatiotemporal coverage to inform these processes, there are limitations as addressed by Clow et al. (2024). For surface ocean pCO_2, the biases and sampling limitations are discussed by Djeutchouang et al. (2022) , highlighting the challenges of sparse coverage.

These findings underscore the need to refine both the physical and biogeochemical components of models to better represent sub-seasonal variability and the complex drivers of productivity in the SO. With this goal in mind, BIOPERIANT12 provides a ~~stable, coherent3–dimensional evolving dataset at relatively high resolution to test sampling strategies and biases~~ coherent, ~~such as investigating the uncertainties in the pin the SO (Djeutchouang et al., 2022) or examining the relationship between cyclonic and anticyclonic eddies in the South Atlantic-SO on heat and carbon (Smith et al., 2023).~~

~~Unfortunately, the computational requirements~~ high-resolution, three-dimensional dataset that is well-suited for understanding upper-ocean physical-biogeochemical processes and interactions on daily to interannual time scales. It has already proven useful for investigate SO sampling biases through observing system simulation experiments (e.g. in air–sea CO_2 flux estimates, Djeutchoua , and to understand role and contributions of mesoscale features in shaping carbon and heat distributions (Smith et al., 2023) . While the computational demands of this configuration ~~with coupled physics-ice-BGC make sensitivity studiesof long duration unrealistic. However, model-observation disagreements provided by BIOPERIANT12 suggest regions where the model configuration was poorly designed or missing processes that warrant further investigation. These will be explored with higher resolution, more appropriate datasets. Some may be addressed with newer versions of the model~~ constrain long-duration sensitivity studies, the insights gained from model–observation mismatches point to specific regions and processes where improvements are needed, and where newer model versions and higher-resolution datasets can help advance our understanding.

Code and data availability. The current version of NEMO is available from the project website: https://www.nemo-ocean.eu under the CeCILL license. The exact version of the model used to produce the results used in this paper is archived on Zenodo (https://doi.org/10.5281/zenodo.13910092), as are input data and scripts to run the model and produce the plots for all the simulations presented in this paper (https://doi.org/10.5281/zenodo.13919282).

Author contributions. Model configuration, production: NC, TCM. Analysis, visualisation, software: NC, SN, MdP, AL, TM. Writing - original draft: NC. Writing, reviewing, editing: all authors.

Competing interests. There are no competing interests to declare.

Acknowledgements. The authors acknowledge their institutional support from the CSIR Parliamentary Grant (0000005278) and the Department of Science and Innovation. SN, NC acknowledges the National Research Foundation South African National Antarctic Programme (SANAP200324510487, SANAP230503101416). PM was also funded by the European Union's Horizon 2020 research 535 and innovation programme under grant agreement No. 820989 (COMFORT). We gratefully acknowledge the Centre for High-Performance Computing (NICIS-CHPC) for providing the computational resources for the development, production, and analysis of BIOPERIANT12. NC extends appreciation to their dedicated team for their invaluable support throughout this challenging process. Additionally, NC has benefited from the expertise and support of A. Albert, J.-M. Molines, and J. Le Sommer at Laboratoire de Glaciologie et Gèophysique de l'Environnement (LGGE), Grenoble through the Marie-Curie International Research Staff Exchange Scheme, SOCCLi (The role of the Southern Ocean Carbon cycle under CLImate change, FP7-PEOPLE-2012-IRSES, 2012-2016).

References

Abernathey, R. P., Cerovecki, I., Holland, P. R., Newsom, E., Mazloff, M., and Talley, L. D.: Water-Mass Transformation by Sea Ice in the Upper Branch of the Southern Ocean Overturning, Nature Geoscience, 9, 596–601, https://doi.org/10.1038/ngeo2749, 2016.

Anav, A., Friedlingstein, P., Kidston, M., Bopp, L., Ciais, P., Cox, P., Jones, C., Jung, M., Myneni, R., and Zhu, Z.: Evaluating the Land and Ocean Components of the Global Carbon Cycle in the CMIP5 Earth System Models, Journal of Climate, 26, 6801–6843, https://doi.org/10.1175/JCLI-D-12-00417.1, 2013.

Aumont, O. and Bopp, L.: Globalizing Results from Ocean in Situ Iron Fertilization Studies, Global Biogeochemical Cycles, 20, https://doi.org/10.1029/2005GB002591, 2006.

Aumont, O., Ethé, C., Tagliabue, A., Bopp, L., and Gehlen, M.: PISCES-v2: An Ocean Biogeochemical Model for Carbon and Ecosystem Studies, Geoscientific Model Development, 8, 2465–2513, https://doi.org/10.5194/gmd-8-2465-2015, 2015.

Bakker, D. C., Pfeil, B., Landa, C. S., Metzl, N., O'Brien, K., Olsen, A., Smith, K., Cosca, C., Harasawa, S., Jones, S. D., et al.: A multi-decade record of high-quality fCO2 data in version 3 of the Surface Ocean CO2 Atlas (SOCAT), Earth System Science Data, 8, 383–413, https://doi.org/10.5194/essd-8-383-2016, 2016.

Barnier, B., Blaker, A., Biatosch, A., Boening, C., Coward, A., Deshayes, J., Hirshi, J., Sommer, J., Madec, G., Maze, G., Molines, J., New, A. L., Penduff, T., Scheinert, M., Talandier, C., and Treguier, A.: DRAKKAR: Developing High Resolution Ocean Components for European Earth System Models, CLIVAR Exchanges, 2014.

Beadling, R. L., Russell, J. L., Stouffer, R. J., Mazloff, M., Talley, L. D., Goodman, P. J., Sallée, J. B., Hewitt, H. T., Hyder, P., and Pandde, A.: Representation of Southern Ocean Properties across Coupled Model Intercomparison Project Generations: CMIP3 to CMIP6, Journal of Climate, 33, 6555–6581, https://doi.org/10.1175/JCLI-D-19-0970.1, 2020.

Bushinsky, S. M., Landschützer, P., Rödenbeck, C., Gray, A. R., Baker, D., Mazloff, M. R., Resplandy, L., Johnson, K. S., and Sarmiento, J. L.: Reassessing Southern Ocean Air-Sea CO $_2$ Flux Estimates With the Addition of Biogeochemical Float Observations, Global Biogeochemical Cycles, 33, 1370–1388, https://doi.org/10.1029/2019GB006176, 2019.

Chapman, C. C.: New Perspectives on Frontal Variability in the Southern Ocean, Journal of Physical Oceanography, 47, 1151–1168, https://doi.org/10.1175/JPO-D-16-0222.1, 2017.

Chassignet, E. P., Yeager, S. G., Fox-Kemper, B., Bozec, A., Castruccio, F., Danabasoglu, G., Horvat, C., Kim, W. M., Koldunov, N., Li, Y., Lin, P., Liu, H., Sein, D. V., Sidorenko, D., Wang, Q., and Xu, X.: Impact of Horizontal Resolution on Global Ocean–Sea Ice Model Simulations Based on the Experimental Protocols of the Ocean Model Intercomparison Project Phase 2 (OMIP-2), Geoscientific Model Development, 13, 4595–4637, https://doi.org/10.5194/gmd-13-4595-2020, 2020.

Clow, G. L., Lovenduski, N. S., Levy, M. N., Lindsay, K., and Kay, J. E.: The Utility of Simulated Ocean Chlorophyll Observations: A Case Study with the Chlorophyll Observation Simulator Package (Version 1) in CESMv2.2, Geoscientific Model Development, 17, 975–995, https://doi.org/10.5194/gmd-17-975-2024, 2024.

Daniault, N. and Ménard, Y.: Eddy Kinetic Energy Distribution in the Southern Ocean from Altimetry and FGGE Drifting Buoys, Journal of Geophysical Research: Oceans, 90, 11 877–11 889, https://doi.org/10.1029/JC090iC06p11877, 1985.

de Boyer Montégut, C., Madec, G., Fischer, A., Lazar, A., and Iudicone, D.: Mixed layer depth over the global ocean: An examination of profile data and a profile-based climatology, Journal of Geophysical Research, 109, 2004.

Dee, D. P., Uppala, S. M., Simmons, A. J., Berrisford, P., Poli, P., Kobayashi, S., Andrae, U., Balmaseda, M. A., Balsamo, G., Bauer, P., Bechtold, P., Beljaars, A. C. M., van de Berg, L., Bidlot, J., Bormann, N., Delsol, C., Dragani, R., Fuentes, M., Geer, A. J., Haim-

berger, L., Healy, S. B., Hersbach, H., Hólm, E. V., Isaksen, L., Kållberg, P., Köhler, M., Matricardi, M., McNally, A. P., Monge-Sanz, B. M., Morcrette, J.-J., Park, B.-K., Peubey, C., de Rosnay, P., Tavolato, C., Thépaut, J.-N., and Vitart, F.: The ERA-Interim Reanalysis: Configuration and Performance of the Data Assimilation System, Quarterly Journal of the Royal Meteorological Society, 137, 553–597, https://doi.org/10.1002/qj.828, 2011.

DeVries, T., Yamamoto, K., Wanninkhof, R., Gruber, N., Hauck, J., Müller, J. D., Bopp, L., Carroll, D., Carter, B., Chau, T.-T.-T., et al.: Magnitude, trends, and variability of the global ocean carbon sink from 1985 to 2018, Global Biogeochemical Cycles, 37, e2023GB007 780, 2023.

Dietze, H., Löptien, U., and Getzlaff, J.: MOMSO 1.0 – an Eddying Southern Ocean Model Configuration with Fairly Equilibrated Natural Carbon, Geoscientific Model Development, 13, 71–97, https://doi.org/10.5194/gmd-13-71-2020, 2020.

Djeutchouang, L. M., Chang, N., Gregor, L., Vichi, M., and Monteiro, P. M. S.: The Sensitivity of pCO_2 Reconstructions to Sampling Scales across a Southern Ocean Sub-Domain: A Semi-Idealized Ocean Sampling Simulation Approach, Biogeosciences, 19, 4171–4195, https://doi.org/10.5194/bg-19-4171-2022, 2022.

Doney, S. C., Lima, I., Moore, J. K., Lindsay, K., Behrenfeld, M. J., Westberry, T. K., Mahowald, N., Glover, D. M., and Takahashi, T.: Skill Metrics for Confronting Global Upper Ocean Ecosystem-Biogeochemistry Models against Field and Remote Sensing Data, Journal of Marine Systems, 76, 95–112, https://doi.org/10.1016/j.jmarsys.2008.05.015, 2009.

Dong, S., Sprintall, J., and Gille, S. T.: Location of the Antarctic Polar Front from AMSR-E Satellite Sea Surface Temperature Measurements, Journal of Physical Oceanography, 36, 2075–2089, https://doi.org/10.1175/JPO2973.1, 2006.

Dong, S., Sprintall, J., Gille, S. T., and Talley, L.: Southern Ocean mixed-layer depth from Argo float profiles, Journal of Geophysical Research: Oceans, 113, https://doi.org/10.1029/2006JC004051, _eprint: https://onlinelibrary.wiley.com/doi/pdf/10.1029/2006JC004051, 2008.

Donohue, K. A., Kennelly, M. A., and Cutting, A.: Sea Surface Height Variability in Drake Passage, Journal of Atmospheric and Oceanic Technology, 33, 669–683, https://doi.org/10.1175/JTECH-D-15-0249.1, 2016.

Downes, S. M., Farneti, R., Uotila, P., Griffies, S. M., Marsland, S. J., Bailey, D., Behrens, E., Bentsen, M., Bi, D., Biastoch, A., Böning, C., Bozec, A., Canuto, V. M., Chassignet, E., Danabasoglu, G., Danilov, S., Diansky, N., Drange, H., Fogli, P. G., Gusev, A., Howard, A., Ilicak, M., Jung, T., Kelley, M., Large, W. G., Leboissetier, A., Long, M., Lu, J., Masina, S., Mishra, A., Navarra, A., George Nurser, A., Patara, L., Samuels, B. L., Sidorenko, D., Spence, P., Tsujino, H., Wang, Q., and Yeager, S. G.: An assessment of Southern Ocean water masses and sea ice during 1988–2007 in a suite of interannual CORE-II simulations, Ocean Modelling, 94, 67–94, https://doi.org/10.1016/j.ocemod.2015.07.022, 2015.

du Plessis, M. D., Swart, S., Biddle, L. C., Giddy, I. S., Monteiro, P. M. S., Reason, C. J. C., Thompson, A. F., and Nicholson, S.-A.: The Daily-Resolved Southern Ocean Mixed Layer: Regional Contrasts Assessed Using Glider Observations, Journal of Geophysical Research: Oceans, 127, e2021JC017 760, https://doi.org/10.1029/2021JC017760, 2022.

Dufour, C. O., Le Sommer, J., Zika, J. D., Gehlen, M., Orr, J. C., Mathiot, P., and Barnier, B.: Standing and Transient Eddies in the Response of the Southern Ocean Meridional Overturning to the Southern Annular Mode, Journal of Climate, 25, 6958–6974, https://doi.org/10.1175/JCLI-D-11-00309.1, 2012.

Dufour, C. O., Sommer, J. L., Gehlen, M., Orr, J. C., Molines, J.-M., Simeon, J., and Barnier, B.: Eddy Compensation and Controls of the Enhanced Sea-to-Air CO $_2$ Flux during Positive Phases of the Southern Annular Mode: CO $_2$ FLUX RESPONSE TO SAM, Global Biogeochemical Cycles, 27, 950–961, https://doi.org/10.1002/gbc.20090, 2013.

Fay, A. R. and McKinley, G. A.: Global Open-Ocean Biomes: Mean and Temporal Variability, Earth System Science Data, 6, 273–284, https://doi.org/10.5194/essd-6-273-2014, 2014.

Fox-Kemper, B., Adcroft, A., B"oning, C. W., Chassignet, E. P., Curchitser, E., Danabasoglu, G., Eden, C., England, M. H., Gerdes, R., Greatbatch, R. J., Griffies, S. M., Hallberg, R. W., Hanert, E., Heimbach, P., Hewitt, H. T., Hill, C. N., Komuro, Y., Legg, S., Le Sommer, J., Masina, S., Marsland, S. J., Penny, S. G., Qiao, F., Ringler, T. D., Treguier, A. M., Tsujino, H., Uotila, P., and Yeager, S. G.: Challenges and Prospects in Ocean Circulation Models, Frontiers in Marine Science, 6, 65, https://doi.org/10.3389/fmars.2019.00065, 2019.

Freeman, N. M. and Lovenduski, N. S.: Mapping the Antarctic Polar Front: weekly realizations from 2002 to 2014, Earth System Science Data, 8, 191–198, https://doi.org/10.5194/essd-8-191-2016, 2016.

Frenger, I., Münnich, M., Gruber, N., and Knutti, R.: Southern Ocean eddy phenomenology, Journal of Geophysical Research: Oceans, 120, 7413–7449, https://doi.org/10.1002/2015JC011047, _eprint: https://onlinelibrary.wiley.com/doi/pdf/10.1002/2015JC011047, 2015.

Frölicher, T. L., Sarmiento, J. L., Paynter, D. J., Dunne, J. P., Krasting, J. P., and Winton, M.: Dominance of the Southern Ocean in Anthropogenic Carbon and Heat Uptake in CMIP5 Models, Journal of Climate, 28, 862–886, https://doi.org/10.1175/JCLI-D-14-00117.1, 2015.

Garcia, H., Locarnini, R., Boyer, T., Antonov, J., Mishonov, A., Baranova, O., Zweng, M., Reagan, J., and Johnson, D.: World Ocean Atlas 2009, Volume 3: Dissolved Oxygen, Apparent Oxygen Utilization, and Oxygen Saturation, 2013.

Garcia, H. E., Locarnini, R. A., Boyer, T. P., Antonov, J. I., Zweng, M. M., Baranova, O. M., and Johnson, D. R.: World Ocean Atlas 2009, Volume 4: Nutrients (Phosphate, Nitrate, and Silicate). S. Levitus, Ed., NOAA Atlas NESDIS 71, Tech. rep., U.S. Government Printing Office, Washington, D.C, 2010.

Gaube, P., J. McGillicuddy Jr., D., and Moulin, A. J.: Mesoscale Eddies Modulate Mixed Layer Depth Globally, Geophysical Research Letters, 46, 1505–1512, https://doi.org/10.1029/2018GL080006, 2019.

Giddy, I., Swart, S., du Plessis, M., Thompson, A. F., and Nicholson, S.-A.: Stirring of Sea-Ice Meltwater Enhances Submesoscale Fronts in the Southern Ocean, Journal of Geophysical Research: Oceans, 126, e2020JC016 814, https://doi.org/10.1029/2020JC016814, _eprint: https://onlinelibrary.wiley.com/doi/pdf/10.1029/2020JC016814, 2021.

Giddy, I. S., Nicholson, S.-A., Queste, B. Y., Thomalla, S., and Swart, S.: Sea-Ice Impacts Inter-Annual Variability of Phytoplankton Bloom Characteristics and Carbon Export in the Weddell Sea, Geophysical Research Letters, 50, e2023GL103 695, https://doi.org/10.1029/2023GL103695, _eprint: https://onlinelibrary.wiley.com/doi/pdf/10.1029/2023GL103695, 2023.

Gray, A. R., Johnson, K. S., Bushinsky, S. M., Riser, S. C., Russell, J. L., Talley, L. D., Wanninkhof, R., Williams, N. L., and Sarmiento, J. L.: Autonomous Biogeochemical Floats Detect Significant Carbon Dioxide Outgassing in the High-Latitude Southern Ocean, Geophysical Research Letters, 45, 9049–9057, https://doi.org/10.1029/2018GL078013, _eprint: https://onlinelibrary.wiley.com/doi/pdf/10.1029/2018GL078013, 2018.

Gregor, L., Lebehot, A. D., Kok, S., and Scheel Monteiro, P. M.: A Comparative Assessment of the Uncertainties of Global Surface Ocean CO_2 Estimates Using a Machine-Learning Ensemble (CSIR-ML6 Version 2019a) – Have We Hit the Wall?, Geoscientific Model Development, 12, 5113–5136, https://doi.org/10.5194/gmd-12-5113-2019, 2019.

Gruber, N., Landschützer, P., and Lovenduski, N. S.: The variable Southern Ocean carbon sink, Annual review of marine science, 11, 159–186, 2019.

Gruber, N., Bakker, D. C. E., DeVries, T., Gregor, L., Hauck, J., Landschützer, P., McKinley, G. A., and Müller, J. D.: Trends and Variability in the Ocean Carbon Sink, Nature Reviews Earth & Environment, 4, 119–134, https://doi.org/10.1038/s43017-022-00381-x, 2023.

Gurvan, M., Bourdallé-Badie, R., Bouttier, P.-A., Bricaud, C., Bruciaferri, D., Calvert, D., Chanut, J., Clementi, E., Coward, A., Delrosso, D., Ethé, C., Flavoni, S., Graham, T., Harle, J., Iovino, D., Lea, D., Lévy, C., Lovato, T., Martin, N., Masson, S., Mocavero, S., Paul, J., Rousset, C., Storkey, D., Storto, A., and Vancoppenolle, M.: NEMO ocean engine, https://doi.org/10.5281/zenodo.1475234, tex.version: v3.4-patch, 2019.

Haarsma, R. J., Roberts, M. J., Vidale, P. L., Senior, C. A., Bellucci, A., Bao, Q., Chang, P., Corti, S., Fučkar, N. S., Guemas, V., von Hardenberg, J., Hazeleger, W., Kodama, C., Koenigk, T., Leung, L. R., Lu, J., Luo, J.-J., Mao, J., Mizielinski, M. S., Mizuta, R., Nobre, P., Satoh, M., Scoccimarro, E., Semmler, T., Small, J., and von Storch, J.-S.: High Resolution Model Intercomparison Project (HighResMIP v1.0) for CMIP6, Geoscientific Model Development, 9, 4185–4208, https://doi.org/10.5194/gmd-9-4185-2016, 2016.

Hague, M. and Vichi, M.: A Link Between CMIP5 Phytoplankton Phenology and Sea Ice in the Atlantic Southern Ocean, Geophysical Research Letters, 45, 6566–6575, https://doi.org/10.1029/2018GL078061, 2018.

Hauck, J., Gregor, L., Nissen, C., Patara, L., Hague, M., Mongwe, P., Bushinsky, S., Doney, S. C., Gruber, N., Le Quéré, C., Manizza, M., Mazloff, M., Monteiro, P. M. S., and Terhaar, J.: The Southern Ocean Carbon Cycle 1985–2018: Mean, Seasonal Cycle, Trends, and Storage, Global Biogeochemical Cycles, 37, e2023GB007 848, https://doi.org/10.1029/2023GB007848, _eprint: https://onlinelibrary.wiley.com/doi/pdf/10.1029/2023GB007848, 2023.

Hewitt, H. T., Roberts, M., Mathiot, P., Biastoch, A., Blockley, E., Chassignet, E. P., Fox-Kemper, B., Hyder, P., Marshall, D. P., Popova, E., Treguier, A.-M., Zanna, L., Yool, A., Yu, Y., Beadling, R., Bell, M., Kuhlbrodt, T., Arsouze, T., Bellucci, A., Castruccio, F., Gan, B., Putrasahan, D., Roberts, C. D., Van Roekel, L., and Zhang, Q.: Resolving and Parameterising the Ocean Mesoscale in Earth System Models, Current Climate Change Reports, 6, 137–152, https://doi.org/10.1007/s40641-020-00164-w, 2020.

Holte, J., Talley, L. D., Gilson, J., and Roemmich, D.: An Argo Mixed Layer Climatology and Database, Geophysical Research Letters, 44, 5618–5626, https://doi.org/10.1002/2017GL073426, 2017.

Kessler, A. and Tjiputra, J.: The Southern Ocean as a Constraint to Reduce Uncertainty in Future Ocean Carbon Sinks, Earth System Dynamics, 7, 295–312, https://doi.org/10.5194/esd-7-295-2016, 2016.

Key, R. M., Kozyr, A., Sabine, C. L., Lee, K., Wanninkhof, R., Bullister, J. L., Feely, R. A., Millero, F. J., Mordy, C., and Peng, T.-H.: A Global Ocean Carbon Climatology: Results from Global Data Analysis Project (GLODAP): GLOBAL OCEAN CARBON CLIMATOLOGY, Global Biogeochemical Cycles, 18, n/a–n/a, https://doi.org/10.1029/2004GB002247, 2004.

Landschützer, P., Gruber, N., Bakker, D. C. E., Stemmler, I., and Six, K. D.: Strengthening seasonal marine CO2 variations due to increasing atmospheric CO2, Nature Climate Change, 8, 146–150, https://doi.org/10.1038/s41558-017-0057-x, number: 2 Publisher: Nature Publishing Group, 2018.

Lauvset, S. K., Key, R. M., Olsen, A., van Heuven, S., Velo, A., Lin, X., Schirnick, C., Kozyr, A., Tanhua, T., Hoppema, M., Jutterström, S., Steinfeldt, R., Jeansson, E., Ishii, M., Perez, F. F., Suzuki, T., and Watelet, S.: A New Global Interior Ocean Mapped Climatology: The 1° × 1° GLODAP Version 2, Earth System Science Data, 8, 325–340, https://doi.org/10.5194/essd-8-325-2016, 2016.

Lecointre, A., Molines, J.-M., and Barnier, B.: Definition of the Interannual Experiment ORCA12.L46-MAL95, 1989-2007, 2011.

Leggett, R. W. and Williams, L. R.: A Reliability Index for Models, Ecological Modelling, 13, 303–312, https://doi.org/10.1016/0304-3800(81)90034-X, 1981.

Lenton, A., Tilbrook, B., Law, R. M., Bakker, D., Doney, S. C., Gruber, N., Ishii, M., Hoppema, M., Lovenduski, N. S., Matear, R. J., McNeil, B. I., Metzl, N., Mikaloff Fletcher, S. E., Monteiro, P. M. S., Rödenbeck, C., Sweeney, C., and Takahashi, T.: Sea–Air CO_2 Fluxes in the Southern Ocean for the Period 1990–2009, Biogeosciences, 10, 4037–4054, https://doi.org/10.5194/bg-10-4037-2013, 2013.

Lévy, M., Mémery, L., and Madec, G.: The onset of a bloom after deep winter convection in the northwestern Mediterranean sea: mesoscale process study with a primitive equation model, Journal of Marine Systems, 16, 7–21, https://doi.org/10.1016/S0924-7963(97)00097-3, 1998.

Lévy, M., Mémery, L., and Madec, G.: The onset of the Spring Bloom in the MEDOC area: mesoscale spatial variability, Deep Sea Research Part I: Oceanographic Research Papers, 46, 1137–1160, https://doi.org/10.1016/S0967-0637(98)00105-8, 1999.

Lévy, M., Klein, P., Tréguier, A.-M., Iovino, D., Madec, G., Masson, S., and Takahashi, K.: Modifications of Gyre Circulation by Sub-Mesoscale Physics, Ocean Modelling, 34, 1–15, https://doi.org/10.1016/j.ocemod.2010.04.001, 2010.

Lévy, M., Resplandy, L., Klein, P., Capet, X., Iovino, D., and Ethé, C.: Grid degradation of submesoscale resolving ocean models: Benefits for offline passive tracer transport, Ocean Modelling, 48, 1–9, 2012.

Locarnini, R. A., Mishonov, A. V., Antonov, J. I., Boyer, T. P., Garcia, H. E., Baranova, O. M., Zweng, M. M., and Johnson, D. R.: World Ocean Atlas 2009, Volume 1: Temperature. S. Levitus, Ed., NOAA Atlas NESDIS 68, Tech. Rep. NOAA Atlas NESDIS 68, U.S. Government Printing Office, Washington, D.C., 2010.

Mackay, N. and Watson, A.: Winter Air-Sea CO2 Fluxes Constructed From Summer Observations of the Polar Southern Ocean Suggest Weak Outgassing, Journal of Geophysical Research: Oceans, 126, e2020JC016 600, https://doi.org/10.1029/2020JC016600, _eprint: https://onlinelibrary.wiley.com/doi/pdf/10.1029/2020JC016600, 2021.

Mahadevan, A., D'Asaro, E., Lee, C., and Perry, M. J.: Eddy-Driven Stratification Initiates North Atlantic Spring Phytoplankton Blooms, Science, 337, 54–58, https://doi.org/10.1126/science.1218740, publisher: American Association for the Advancement of Science, 2012.

Marshall, J., Jones, H., Karsten, R., and Wardle, R.: Can Eddies Set Ocean Stratification?, Journal of Physical Oceanography, 32, 26–38, https://doi.org/10.1175/1520-0485(2002)032<0026:CESOS>2.0.CO;2, publisher: American Meteorological Society Section: Journal of Physical Oceanography, 2002.

Meier, W. N., Fetterer, F., Savoie, M., Mallory, S., Duerr, R., and Stroeve, J.: NOAA/NSIDC Climate Data Record of Passive Microwave Sea Ice Concentration, Version 3, https://doi.org/10.7265/N59P2ZTG, 2017.

Meijers, A. J. S.: The Southern Ocean in the Coupled Model Intercomparison Project Phase 5, Philosophical Transactions of the Royal Society A: Mathematical, Physical and Engineering Sciences, 372, 20130 296, https://doi.org/10.1098/rsta.2013.0296, 2014.

Meredith, M. P., Schofield, O., Newman, L., Urban, E., and Sparrow, M.: The Vision for a Southern Ocean Observing System, Current Opinion in Environmental Sustainability, 5, 306–313, https://doi.org/10.1016/j.cosust.2013.03.002, 2013.

Mongwe, N. P., Chang, N., and Monteiro, P. M. S.: The Seasonal Cycle as a Mode to Diagnose Biases in Modelled CO2 Fluxes in the Southern Ocean, Ocean Modelling, 106, 90–103, https://doi.org/10.1016/j.ocemod.2016.09.006, 2016.

Mongwe, N. P., Vichi, M., and Monteiro, P. M. S.: The Seasonal Cycle of pCO_2 and CO_2 Fluxes in the Southern Ocean: Diagnosing Anomalies in CMIP5 Earth System Models, Biogeosciences, 15, 2851–2872, https://doi.org/10.5194/bg-15-2851-2018, 2018.

Monteiro, P. M. S., Gregor, L., Lévy, M., Maenner, S., Sabine, C. L., and Swart, S.: Intraseasonal variability linked to sampling alias in air-sea CO2 fluxes in the Southern Ocean, Geophysical Research Letters, 42, 8507–8514, https://doi.org/10.1002/2015GL066009, _eprint: https://onlinelibrary.wiley.com/doi/pdf/10.1002/2015GL066009, 2015.

Munday, D. R., Johnson, H. L., and Marshall, D. P.: Impacts and Effects of Mesoscale Ocean Eddies on Ocean Carbon Storage and Atmospheric pCO2, Global Biogeochemical Cycles, 28, 877–896, https://doi.org/10.1002/2014GB004836, 2014.

Munday, D. R., Zhai, X., Harle, J., Coward, A. C., and Nurser, A. J. G.: Relative vs. Absolute Wind Stress in a Circumpolar Model of the Southern Ocean, Ocean Modelling, 168, 101 891, https://doi.org/10.1016/j.ocemod.2021.101891, 2021.

NEMO Consortium: NEMO Reference configurations inputs, https://doi.org/10.5281/zenodo.3767939, 2020.

Nicholson, S.-A., Lévy, M., Jouanno, J., Capet, X., Swart, S., and Monteiro, P. M. S.: Iron Supply Pathways Between the Surface and Subsurface Waters of the Southern Ocean: From Winter Entrainment to Summer Storms, Geophysical Research Letters, 46, 14 567–14 575, https://doi.org/10.1029/2019GL084657, 2019.

Nicholson, S.-A., Whitt, D. B., Fer, I., du Plessis, M. D., Lebéhot, A. D., Swart, S., Sutton, A. J., and Monteiro, P. M. S.: Storms Drive Outgassing of CO2 in the Subpolar Southern Ocean, Nature Communications, 13, 158, https://doi.org/10.1038/s41467-021-27780-w, 2022.

Olsen, A., Key, R. M., van Heuven, S., Lauvset, S. K., Velo, A., Lin, X., Schirnick, C., Kozyr, A., Tanhua, T., Hoppema, M., Jutterström, S., Steinfeldt, R., Jeansson, E., Ishii, M., Pérez, F. F., and Suzuki, T.: The Global Ocean Data Analysis Project Version 2 (GLODAPv2) – an Internally Consistent Data Product for the World Ocean, Earth System Science Data, 8, 297–323, https://doi.org/10.5194/essd-8-297-2016, 2016.

Orsi, A. H., Whitworth, T., and Nowlin, W. D.: On the Meridional Extent and Fronts of the Antarctic Circumpolar Current, Deep Sea Research Part I: Oceanographic Research Papers, 42, 641–673, https://doi.org/10.1016/0967-0637(95)00021-W, 1995.

Patara, L., Böning, C. W., and Biastoch, A.: Variability and Trends in Southern Ocean Eddy Activity in 1/12° Ocean Model Simulations: Changes in Southern Ocean Eddy Activity, Geophysical Research Letters, 43, 4517–4523, https://doi.org/10.1002/2016GL069026, 2016.

Peng, G., Meier, W. N., Scott, D. J., and Savoie, M. H.: A Long-Term and Reproducible Passive Microwave Sea Ice Concentration Data Record for Climate Studies and Monitoring, Earth System Science Data, 5, 311–318, https://doi.org/10.5194/essd-5-311-2013, 2013.

Renault, L., Molemaker, M. J., McWilliams, J. C., Shchepetkin, A. F., Lemarié, F., Chelton, D., Illig, S., and Hall, A.: Modulation of Wind Work by Oceanic Current Interaction with the Atmosphere, Journal of Physical Oceanography, 46, 1685–1704, https://doi.org/10.1175/JPO-D-15-0232.1, 2016.

Rieck, J. K., Böning, C. W., Greatbatch, R. J., and Scheinert, M.: Seasonal Variability of Eddy Kinetic Energy in a Global High-Resolution Ocean Model: ANNUAL CYCLE OF EDDY KINETIC ENERGY, Geophysical Research Letters, 42, 9379–9386, https://doi.org/10.1002/2015GL066152, 2015.

Rintoul, S. R.: The Global Influence of Localized Dynamics in the Southern Ocean, Nature, 558, 209–218, https://doi.org/10.1038/s41586-018-0182-3, 2018.

Rodgers, K. B., Schwinger, J., Fassbender, A. J., Landschützer, P., Yamaguchi, R., Frenzel, H., Stein, K., Müller, J. D., Goris, N., Sharma, S., et al.: Seasonal variability of the surface ocean carbon cycle: A synthesis, Global Biogeochemical Cycles, 37, e2023GB007 798, 2023.

Rohr, T., Harrison, C., Long, M. C., Gaube, P., and Doney, S. C.: Eddy-Modified Iron, Light, and Phytoplankton Cell Division Rates in the Simulated Southern Ocean, Global Biogeochemical Cycles, 34, e2019GB006 380, https://doi.org/10.1029/2019GB006380, 2020.

Rosso, I., Mazloff, M. R., Talley, L. D., Purkey, S. G., Freeman, N. M., and Maze, G.: Water Mass and Biogeochemical Variability in the Kerguelen Sector of the Southern Ocean: A Machine Learning Approach for a Mixing Hot Spot, Journal of Geophysical Research: Oceans, 125, e2019JC015 877, https://doi.org/10.1029/2019JC015877, 2020.

Russell, J. L., Kamenkovich, I., Bitz, C., Ferrari, R., Gille, S. T., Goodman, P. J., Hallberg, R., Johnson, K., Khazmutdinova, K., Marinov, I., Mazloff, M., Riser, S., Sarmiento, J. L., Speer, K., Talley, L. D., and Wanninkhof, R.: Metrics for the Evaluation of the Southern Ocean in Coupled Climate Models and Earth System Models, Journal of Geophysical Research: Oceans, 123, 3120–3143, https://doi.org/10.1002/2017JC013461, 2018.

Rustogi, P., Landschützer, P., Brune, S., and Baehr, J.: The impact of seasonality on the annual air-sea carbon flux and its interannual variability, npj Climate and Atmospheric Science, 6, 66, 2023.

Ryan-Keogh, T. J., Thomalla, S. J., Chang, N., and Moalusi, T.: A new global oceanic multi-model net primary productivity data product, Earth System Science Data, 15, 4829–4848, 2023.

Sallée, J.-B., Shuckburgh, E., Bruneau, N., Meijers, A. J. S., Bracegirdle, T. J., Wang, Z., and Roy, T.: Assessment of Southern Ocean water mass circulation and characteristics in CMIP5 models: Historical bias and forcing response, Journal of Geophysical Research: Oceans, 118, 1830–1844, https://doi.org/10.1002/jgrc.20135, _eprint: https://onlinelibrary.wiley.com/doi/pdf/10.1002/jgrc.20135, 2013.

Sathyendranath, S., Brewin, R. J. W., Brockmann, C., Brotas, V., Calton, B., Chuprin, A., Cipollini, P., Couto, A. B., Dingle, J., Doerffer, R., Donlon, C., Dowell, M., Farman, A., Grant, M., Groom, S., Horseman, A., Jackson, T., Krasemann, H., Lavender, S., Martinez-Vicente, V., Mazeran, C., Mélin, F., Moore, T. S., Müller, D., Regner, P., Roy, S., Steele, C. J., Steinmetz, F., Swinton, J., Taberner, M., Thompson, A., Valente, A., Zühlke, M., Brando, V. E., Feng, H., Feldman, G., Franz, B. A., Frouin, R., Gould, R. W., Hooker, S. B., Kahru, M., Kratzer, S., Mitchell, B. G., Muller-Karger, F. E., Sosik, H. M., Voss, K. J., Werdell, J., and Platt, T.: An Ocean-Colour Time Series for Use in Climate Studies: The Experience of the Ocean-Colour Climate Change Initiative (OC-CCI), Sensors, 19, 4285, https://doi.org/10.3390/s19194285, 2019.

Séférian, R., Bopp, L., Gehlen, M., Orr, J. C., Ethé, C., Cadule, P., Aumont, O., Salas y Mélia, D., Voldoire, A., and Madec, G.: Skill Assessment of Three Earth System Models with Common Marine Biogeochemistry, Climate Dynamics, 40, 2549–2573, https://doi.org/10.1007/s00382-012-1362-8, 2013.

Shao, A. E., Gille, S. T., Mecking, S., and Thompson, L.: Properties of the Subantarctic Front and Polar Front from the Skewness of Sea Level Anomaly: PROPERTIES OF THE SAF AND PF, Journal of Geophysical Research: Oceans, 120, 5179–5193, https://doi.org/10.1002/2015JC010723, 2015.

Smith, T., Nicholson, S., Engelbrecht, F., Chang, N., Mongwe, N., and Monteiro, P.: The Heat and Carbon Characteristics of Modeled Mesoscale Eddies in the South–East Atlantic Ocean, Journal of Geophysical Research: Oceans, 128, https://doi.org/10.1029/2023JC020337, 2023.

Song, H., Long, M. C., Gaube, P., Frenger, I., Marshall, J., and McGillicuddy Jr., D. J.: Seasonal Variation in the Correlation Between Anomalies of Sea Level and Chlorophyll in the Antarctic Circumpolar Current, Geophysical Research Letters, 45, 5011–5019, https://doi.org/10.1029/2017GL076246, 2018.

Swart, S., Chang, N., Fauchereau, N., Joubert, W., Lucas, M., Mtshali, T., Roychoudhury, A., Tagliabue, A., Thomalla, S., and Waldron, H.: Southern Ocean Seasonal Cycle Experiment 2012: Seasonal Scale Climate and Carbon Cycle Links, South African Journal of Science, 108, 11–13, 2012.

Tagliabue, A., Mtshali, T., Aumont, O., Bowie, A. R., Klunder, M. B., Roychoudhury, A. N., and Swart, S.: A Global Compilation of Dissolved Iron Measurements: Focus on Distributions and Processes in the Southern Ocean, Biogeosciences, 9, 2333–2349, https://doi.org/10.5194/bg-9-2333-2012, 2012.

Tagliabue, A., Sallée, J.-B., Bowie, A. R., Lévy, M., Swart, S., and Boyd, P. W.: Surface-water iron supplies in the Southern Ocean sustained by deep winter mixing, Nature Geoscience, 7, 314–320, https://doi.org/10.1038/ngeo2101, number: 4 Publisher: Nature Publishing Group, 2014.

Tagliabue, A., Aumont, O., DeAth, R., Dunne, J. P., Dutkiewicz, S., Galbraith, E., Misumi, K., Moore, J. K., Ridgwell, A., Sherman, E., Stock, C., Vichi, M., Völker, C., and Yool, A.: How Well Do Global Ocean Biogeochemistry Models Simulate Dissolved Iron Distributions?, Global Biogeochemical Cycles, 30, 149–174, https://doi.org/10.1002/2015GB005289, 2016.

Thomalla, S. J., Fauchereau, N., Swart, S., and Monteiro, P. M. S.: Regional Scale Characteristics of the Seasonal Cycle of Chlorophyll in the Southern Ocean, Biogeosciences, 8, 2849–2866, https://doi.org/10.5194/bg-8-2849-2011, 2011.

Thomalla, S. J., Nicholson, S.-A., Ryan-Keogh, T. J., and Smith, M. E.: Widespread changes in Southern Ocean phytoplankton blooms linked to climate drivers, Nature Climate Change, 13, 975–984, https://doi.org/10.1038/s41558-023-01768-4, number: 9 Publisher: Nature Publishing Group, 2023.

Toolsee, T., Nicholson, S.-A., and Monteiro, P. M. S.: Storm-Driven pCO2 Feedback Weakens the Response of Air-Sea CO2 Fluxes in the Sub-Antarctic Southern Ocean, Geophysical Research Letters, 51, e2023GL107 804, https://doi.org/10.1029/2023GL107804, 2024.

Treguier, A. M., de Boyer Montégut, C., Bozec, A., Chassignet, E. P., Fox-Kemper, B., McC. Hogg, A., Iovino, D., Kiss, A. E., Le Sommer, J., Li, Y., Lin, P., Lique, C., Liu, H., Serazin, G., Sidorenko, D., Wang, Q., Xu, X., and Yeager, S.: The mixed-layer depth in the Ocean Model Intercomparison Project (OMIP): impact of resolving mesoscale eddies, Geoscientific Model Development, 16, 3849–3872, https://doi.org/10.5194/gmd-16-3849-2023, publisher: Copernicus GmbH, 2023.

Uchida, T., Balwada, D., Abernathey, R., McKinley, G., Smith, S., and Lévy, M.: The Contribution of Submesoscale over Mesoscale Eddy Iron Transport in the Open Southern Ocean, Journal of Advances in Modeling Earth Systems, 11, 3934–3958, https://doi.org/10.1029/2019MS001805, 2019.

Uchida, T., Balwada, D., P. Abernathey, R., A. McKinley, G., K. Smith, S., and Lévy, M.: Vertical Eddy Iron Fluxes Support Primary Production in the Open Southern Ocean, Nature Communications, 11, 1125, https://doi.org/10.1038/s41467-020-14955-0, 2020.

Verdy, A. and Mazloff, M. R.: A Data Assimilating Model for Estimating Southern Ocean Biogeochemistry, Journal of Geophysical Research: Oceans, 122, 6968–6988, https://doi.org/10.1002/2016JC012650, 2017.

Wang, J., Mazloff, M. R., and Gille, S. T.: The Effect of the Kerguelen Plateau on the Ocean Circulation, Journal of Physical Oceanography, 46, 3385–3396, https://doi.org/10.1175/JPO-D-15-0216.1, 2016.

Whitt, D. B., Lévy, M., and Taylor, J. R.: Submesoscales Enhance Storm-Driven Vertical Mixing of Nutrients: Insights From a Biogeochemical Large Eddy Simulation, Journal of Geophysical Research: Oceans, 124, 8140–8165, https://doi.org/10.1029/2019JC015370, 2019.

Whitworth, T. and Peterson, R. G.: Volume Transport of the Antarctic Circumpolar Current from Bottom Pressure Measurements, Journal of Physical Oceanography, 15, 810–816, https://doi.org/10.1175/1520-0485(1985)015<0810:VTOTAC>2.0.CO;2, 1985.

Williams, N. L., Juranek, L. W., Feely, R. A., Russell, J. L., Johnson, K. S., and Hales, B.: Assessment of the Carbonate Chemistry Seasonal Cycles in the Southern Ocean From Persistent Observational Platforms, Journal of Geophysical Research: Oceans, 123, 4833–4852, https://doi.org/10.1029/2017JC012917, 2018.